JPRS L/9308

19 September 1980

USSR Report

PHYSICS AND MATHEMATICS

(FOUO 8/80)

FBIS FOREIGN BROADCAST INFORMATION SERVICE

NOTE

JPRS publications contain information primarily from foreign newspapers, periodicals and books, but also from news agency transmissions and broadcasts. Materials from foreign-language sources are translated; those from English-language sources are transcribed or reprinted, with the original phrasing and other characteristics retained.

Headlines, editorial reports, and material enclosed in brackets [] are supplied by JPRS. Processing indicators such as [Text] or [Excerpt] in the first line of each item, or following the last line of a brief, indicate how the original information was processed. Where no processing indicator is given, the information was summarized or extracted.

Unfamiliar names rendered phonetically or transliterated are enclosed in parentheses. Words or names preceded by a question mark and enclosed in parentheses were not clear in the original but have been supplied as appropriate in context. Other unattributed parenthetical notes within the body of an item originate with the source. Times within items are as given by source.

The contents of this publication in no way represent the policies, views or attitudes of the U.S. Government.

For further information on report content call (703) 351-2938 (economic); 3468 (political, sociological, military); 2726 (life sciences); 2725 (physical sciences).

APPROVED FOR RELEASE: 2007/02/08: CIA-RDP82-00850R000300030028-5

JPRS L/9308

19 September 1980

USSR REPORT

PHYSICS AND MATHEMATICS

(FOUO 8/80)

CONTENTS

ACOUSTICS

PRINCIPLES OF ULTRASONIC PHYSICS

Leningrad OSNOVY FIZIKI UL'TRAZVUKA in Russian 1980 signed to press 12 Oct 79

[Annotation and table of contents from a textbook by Vladimir Aleksandrovich Shutilov, Leningrad University, 3269 copies, 280 pages]

[Text] This book considers the propagation of ultrasonic waves in liquids, gases, and solids, which are treated as continuous media with different elastic properties. Problems having a direct relationship to specific ultrasonic characteristics are presented systematically: possibilities of generating directional plane wave beams, high-intensity ultrasonic radiation, etc. In the book most of the attention is focused on different aspects of the propagation of plane waves: their general characteristics, damping, scattering by inhomogeneities, reflection, refraction, transmission through layers, interference, diffraction, analysis of nonlinear phenomena, pondermotive forces, and edge and other effects in bounded beams. Attention is also paid to spherical waves which are formed by pulsed vibrations of spherical bodies, in the far zone of small radiators, and in ultrasonic focusing systems. Most of these problems are discussed in regard to longitudinal waves in media having bulk elasticity and for other types of waves, in particular, for shear waves in liquids and solids; additional attention is given to problems involving their specific properties. This includes boundary and nonlinear effects in solids, transformation of waves, their dispersion, surface waves, and the relationships between sonic velocities and elastic moduli in crystals, including piezoelectric crystals.

This texbook is designed for students in the upper grades and for post-graduate students in the physics departments of universities and institutes, and it will be useful also for scientists and technicians specializing in different branches of ultrasonics.

TABLE OF CONTENTS

9370
CSO: 1862

CLASSICIAL MECHANICS

GYROSTABILIZERS OF INERTIAL CONTROL SYSTEMS

Leningrad GIROSTABILIZATORY INERTSIAL'NYKH SISTEM UPRAVLENIYA (Gyrostabilizers of Inertial Control Systems) in Russian 1979 signed to press 19 Feb 79 pp 2-4, 143-150

[Annotation, Foreword, References and Table of Contents from book by Leonid Anatol'yevich Severov, Izdatel'stvo Leningradskogo universiteta, 924 copies, 151 pages]

[Text] Gyrostabilizers of noncorrecting inertial control systems for unmanned spacecraft are considered in the book. Main attention is devoted to problems of analysis and synthesis of the platform stabilization circuit. Kinematic and dynamic description of gyrostabilizers with different platform gimbal suspension circuits, distinguished by methods of arranging the gyroscopes and the stabilizing motors, is presented. The problem of analytical design of practically realized optimum gyrostabilizer controllers is posed and solved. The possibility of achieving high amplification factors in the stabilizing circuit is analyzed both from positions of the structural conditions of the stability of a linear multidimensional system and from the condition of the absolute stability of the system with standard nonlinear components.

The book is intended for specialists engaged in design of gyrostabilizers and may also be useful to students and postgraduate students majoring in certain fields.

Foreword

Modern self-contained inertial control systems (ISU) for spacecraft are constructed with gyroscopic stabilization of the inertial sensing elements, which is most frequently accomplished by using a three-axis gyroscopic stabilizer (TGS) [1-5].

Inertial orientation of the TGS platform is usually employed in ISU. The short operating time of the system permits construction of closed type ISU [6]. Variation of the gravity acceleration components during flight is taken into account with more accurate solution of the control problem [1].

It follows from the foregoing that the ISU error will include the errors introduced by the TGS. Therefore, special attention is devoted in design of TGS to solution of two main problems: 1) high-precision initial deployment of the platform with initial sensing elements and 2) ensuring precise inertial orientation of the platform during flight.

It must be noted that TGS of the considered type operate under intensive vibration and load conditions during flight. This considerably complicates solution of the second main problem and requires construction of a platform stabilization circuit with high amplification factors and adoption of special measures to reduce instrument drift of the platform [4].

The problems of analysis and design of a platform stabilization system are mainly outlined in the given monograph. A mathematical model of a multidimensional stabilization system is developed which takes into account elastic deformation of the components, typical nonlinearities, different schemes for arranging the gyroscopes and stabilizing motors. The composition of perturbing effects is analyzed and the problem of analytical design of practically realized optimum TGS controllers for inertial control systems is posed and solved. The possibility of realizing high amplification factors in the stabilization system is analyzed both from the position of the structural conditions of the stability of TGS constructed on two-degree gyroscopes and from conditions of the absolute stability of a multidimensional nonlinear system containing typical nonlinearities of the elements.

The author hopes that the proposed book will be useful in solution of problems of designing TGS for inertial control systems.

BIBLIOGRAPHY

1. Ishlinskiy, A. U., "Inertsial'noye upravleniye ballisticheskimi raketami" [Inertial Control of Ballistic Missiles], Moscow, Nauka, 1968.

2. Nazarov, B. I., "Power Gyrostabilizers," in "Razvitiye mekhaniki giroskopicheskikh i inertsial'nykh sistem" [Developing the Mechanics of Gyroscopic and Inertial Systems], Moscow, 1973.

3. "Giroskopicheskiye sistemy. Proyektirovaniye giroskopicheskikh sistem" [Gyroscopic Systems. Designing Gyroscopic Systems], edited by D. S. Pel'por, Parts 1 and 2, Moscow, 1977.

4. "Inertsial'nyye sistemy upravleniya" [Inertial Control Systems], edited by D. Pitman, Moscow, 1964.

5. "Inertsial'naya navigatsiya" [Inertial Navigation], edited by K. F. O'Donnel, Moscow, 1969.

6. Fridlender, G. O., "Inertsial'nyye sistemy navigatsii" [Inertial Navigation Systems], Moscow, 1961.

7. Pel'por, D. S., "Giroskopicheskiye sistemy" [Gyroscopic Systems], Moscow, 1971.

8. "Giroskopicheskiye sistemy" [Gyroscopic Systems], edited by L. A. Severov, Leningrad, 1975.

9. Ishlinskiy, A. Yu., "Oriyentatsiya, giroskopy i inertsial'naya navigatsiya" [Orientation, Gyroscopes and Inertial Navigation], Moscow, 1976.

10. Maunder, L., "Problems of the Dynamics of Gyroscope Gimbal Suspension," in "Problemy giroskopii" [Problems of Gyroscopy], Moscow, 1967.

11. Ponyrko, S. A. and L. A. Severov, "Engineering Methods of Compiling Equations of Motion of a Three-Axis Gyrostabilizer," TRUDY LIAP.

12. Besekerskiy, V. A. and Ye. A. Fabrikant, "Dinamicheskiy sintez sistem giroskopicheskoy stabilizatsii" [Dynamic Synthesis of Gyrostabilizing Systems], Leningrad, 1968.

13. Brokmeyster, I. F., "Sistemy inertsial'noy navigatsii" [Inertial Navigation Systems], Leningrad, 1967.

14. Rivkin, S. S., "Application of the Method of Matrix Theory to Analysis of the Configuration of Gyroscopic Devices," in "Voprosy prikladnoy giroskopii" [Problems of Applied Gyroscopy], second edition, Leningrad, 1960.

15. Roytenberg, Ya. N., "Giroskopy" [Gyroscopes], Moscow, 1966.

16. Lur'ye, L. I., "Analiticheskaya mekhanika" [Analytical Mechanics], Moscow, 1961.

17. Butenin, N. V., "Vvedeniye v analiticheskuyu mekhaniku" [Introduction to Analytical Mechanics], Moscow, 1971.

18. Arnol'd, R. N. and L. Monder, "Girodinamika i yeye tekhnicheskoye primeneniye" [Gyrodynamics and Its Engineering Applications], Moscow, 1964.

19. Savant, S. J. et al, "Printsipy inertsial'noy navigatsii" [Principles of Inertial Navigation], Moscow, 1965.

20. Safarov, R. G., "Analyzing the Stability of a Three-Axis Gyrostabilizer With Additional Frame," in "Sbornik nauchnykh trudov PLI" [Collection of Scientific Papers of the PLI], No 47, Perm', 1968.

21. MacClure, K. L., "Teoriya inertsial'noy navigatsii" [Inertial Navigation Theory], Moscow, 1964.

22. El'sgol'ts, L. E., "Differentsial'nyye uravneniya i variatsionnoye ischisleniye" [Differential Equations and Variational Calculus], Moscow, 1969.

23. Syu, D. and A. Meyer, "Sovremennaya teoriya avtomaticheskogo upravleniya i yeye primeneniye" [Modern Theory of Automatic Control and Application of It], Moscow, 1972.

24. Pukhov, R. Ye., G. I. Grezdov and A. F. Verlan', "Metody resheniya krayevykh zadach na elektronnykh modelyakh" [Methods of Solving Boundary-Value Problems on Electronic Models], Kiev, 1965.

25. Berezin, I. S. and N. G. Zhidkov, "Metody vychisleniya" [Methods of Calculation], Moscow, 1966.

26. Severov, L. A. and G. M. Bykova, "Optimum Control of the Additional Ring Motor in a Three-Axis Gyrostabilizer With Arbitrary Motion of the Object," in "Prikladnaya giroskopiya" [Applied Gyroscopy], Izd-vo Leningradskogo universiteta, 1974.

27. Bykova, G. M. and L. A. Severov, "Optimizing the Kinematic Characteristics of the Gimbal Suspensions of Three-Axis Gyrostabilizers With Additional Degrees of Freedom," IZV. VYSSH. UCHEB. ZAVEDENIY, PRIBOROSTROYENIYE, Vol 20, No 6, 1977.

28. Nazarov, B. I., "Gyrostabilizer Errors," IZV. AN SSSR, OTN., TEKHNICHESKAYA KIBERNETIKA, No 2, 1963.

29. Rivkin, S. S., "Investigating Ship Gyroscopic Devices With Irregular Heeling of the Vessel," in "Pervaya Mezhvuzovskaya Nauchno-Tekhnicheskaya konferentsiya po problemam sovremennoy giroskopii" [The First Intervuz Scientific and Technical Conference on Problems of Modern Gyroscopy], Leningrad, 1960.

30. Kuzovkov, N. T., "The Stability of Power Gyrostabilizers With Large Angles of Deflection," IZV. AN SSSR, OTN., TEKHNICHESKAYA KIBERNETIKA, No 1, 1958.

31. Pel'por, D. S., Yu. A. Kolosov and Ye. R. Rakhteyenko, "Raschet i proyektirovaniye giroskopicheskikh stabilizatorov" [Calculation and Design of Gyrostabilizers], Moscow, 1972.

32. Severov, L. A., "Problems of the Dynamics of a Three-Axis Gyrostabilizer," in "Problemy povysheniya tochnosti i nadezhnosti giroskopicheskikh sistem" [Problems of Increasing the Accuracy and Reliability of Gyroscopic Systems], Leningrad, 1967.

33. Severov, L. A. and P. B. Dergachev, "Orientation of Gyroscopes on a Three-Axis Gyrostabilizer Platform," TRUDY LIAP, No 60, 1969.

34. Astrom, K. J., "Analysis and Synthesis of Inertial Platforms With Single-Axis Gyroscopes," Goteborg, 1919.

35. Nazarov, B. I., "The Dynamic Drift of Gyroscopic Devices With Random Perturbations," in "Problemy povysheniya tochnosti i nadezhnosti giroskopicheskikh sistem," Leningrad, 1967.

36. Novozhilov, I. V., "The Working Principle of a Three-Axis Gyrostabilizer," IZV. AN SSSR, MEKHANIKA, No 5, 1965.

37. Shilinskiy, A. Yu., "Mekhanika giroskopicheskikh sistem" [The Mechanics of Gyroscopic Systems], Moscow, 1963.

38. Shilinskiy, A. Yu., "One Mechanical Analogy of a Gyrostabilizer in the Presence of the Elastic Pliancy of Its Components," DOKL. AN SSSR, Vol 161, No 6, 1965.

39. Severov, L. A., "Calculating the Stability of Gyroscope Frames With Regard to the Elastic Pliability of Some Components of the Gyroscope Suspension," IZV. VYSSH. UCHEB. ZAVEDENIY, PRIBOROSTROYENIYE, No 6, 1963.

40. Morozovskiy, V. T., "Mnogosvyzannyye sistemy avtomaticheskogo regulirovaniya" [Multiply Connected Automatic Control Systems], Moscow, 1970.

41. Letov, A. M., "Analytical Design of Regulators," AVTOMATIKA I TELEMEKHANIKA, Vol 21, No 4-6, 1960; Vol 22, No 4, 1961.

42. Aleksandrov, A. G., "Analytical Design of an Optimum Gyroframe Regulator Installed on a Movable Base," AVTOMATIKA I TELEMEKHANIKA, No 12, 1967.

43. Abramov, A. I. and I. B. Berlin, "Synthesis of the Optimum Control Part of a Power Gyrostabilizer," AVTOMATIKA I TELEMEKHANIKA, No 8, 1970.

44. Shandon, S. L. and Chang, "Sintez optimal'nykh sistem avtomaticheskogo upravleniya" [Synthesis of Optimum Automatic Control Systems], Moscow, 1964.

45. Larin, V. B., K. I. Naumenko and V. N. Suntsev, "Sintez optimal'nykh lineynykh sistem s obratnoy svyaz'yu" [Synthesis of Optimum Linear Systems With Feedback], Kiev, 1973.

46. Yanushevskiy, R. T., "Teoriya lineynykh optimal'nykh mnogosvyzannykh sistem upravleniya" [The Theory of Linear Optimum Multiply Connected Control Systems], Moscow, 1973.

47. Nazarov, B. I. and G. A. Khlebnikov, "Girostabilizatory raket" [Missile Gyrostabilizers], Moscow, 1975.

48. "Navigatsiya, navedeniye i stabilizatsiya v kosmose" [Navigation, Guidance and Stabilization in Space], edited by D. E. Miller, Moscow, 1970.

49. Sinitsin, I. N. and L. N. Slezkin, "Linear-Acceleration Gyrostabilizers" in "Razvitiye mekhaniki giroskopicheskikh i inertsial'nykh sistem" [Developing the Mechanics of Gyroscopic and Inertial Systems], Moscow, 1973.

50. Livshitz, N. A. and V. N. Pugachev, "Veroyatnostnyy analiz sistem avtomaticheskogo upravleniya" [Probability Analysis of Automatic Control Systems], Parts 1 and 2, Moscow, 1963.

51. Reising, H. and T. Angelize, "Measuring Apparatus for Investigating the Phenomenon of Unstable Combustion," in "Issledovaniye raketnykh dvigateley na zhidkom toplive" [Investigating Liquid-Fuel Rocket Engines], Moscow, 1964.

52. Pitman, J. and R. Goodson, "The Behavior of Gyroscopic Instruments Subjected to Random Vibrations," in "Problemy giroskopii," Moscow, 1967.

53. Roytenberg, Ya. N., "Avtomaticheskoye upravleniye" [Automatic Control], Moscow, 1971.

54. Solodovnikov, V. V. and V. L. Lenskiy, "Synthesis of Control Systems of Minimum Complexity," IZV. AN SSSR, TEKHNICHESKAYA KIBERNETIKA, No 2, 1966.

55. Solodovnikov, V. V., "The Principle of Minimum Complexity and Its Application for Regulating Problems of Optimum Stochastic Control," IZV. VYS. UCHEB. ZAVEDENIY, PRIBOROSTROYENIYE, Vol 13, No 3, 1970.

56. Kalman, R. E., "When Is A Linear Central System Optimal?" in "Joint Autom. Contr. Conf.,"Minnesota, 1963.

57. Dech, H., "Rukovodstvo k prakticheskomu primeneniyu preobrazovaniya Laplasa" [Handbook for Practical Application of Laplace Transforms], Moscow, 1965.

58. Gantmacher, F. R., "Teoriya matrits" [Matrix Theory], Moscow, 1967.

59. Sveshnikov, A. G. and A. N. Tikhonov, "Teoriya funktsiy kompleksnoy peremennoy" [Theory of Complex Variable Functions], Moscow, 1970.

60. Sveshnikov, A. G., "Prikladnyye metody teorii sluchaynykh funktsiy" [Applied Methods of Random Function Theory], Moscow, 1968.

61. Davis, M. C., "On Factoring theSpectral Matrix," in "Joint Autom. Contr. Conf., " Minnesota, 1963.

62. "Sovremennaya teoriya sistem upravleniya" [Modern Theory of Control Systems], edited by K. T. Leondes, Moscow, 1970.

63. Lunts, Ya. L., "Oshibki giroskopicheskikh priborov" [Errors of Gyroscopic Devices], Leningrad, 1968.

64. Severov, L. A. and Yu. A. Taran, "The Drifts of a Three-Axis Static Tyrostabilizer Exposed to Random External Perturbations on One Stabilization Axis," IZV. VYS. UCHEB. ZAVEDENIY, PRIBOROSTROYENIYE, Vol 12, No 4, 1969.

65. Ishlinskiy, A. Yu., "The Lower Stability of a Two-Axis Gyrostabilizer Compared to a One-Axis Stabilizer," DOKL. AN SSSR, No 6, 1965.

66. Karpov, V. N., "The Dynamics of a Three-Axis Gyrostabilizer," IZV. VYS. UCHEB. ZAVEDENIY, PRIBOROSTROYENIYE, No 5, 1964.

67. Slezkin, L. N. and Dang-Zhi,Wang, "The Effect of Relationships Between the Filaments of a Gyroscopic Platform," IZV. VYS. UCHEB. ZAVEDENIY, PRIBOROSTROYENIYE, No 4, 1965.

68. Severov, L. A., "The Effect of Gimbal Suspension Inertia on the Stability of a Spatial Gyroscope Frame on Floating Integrating Gyroscopes," TRUDY LIAP, No 40, 1963.

69. Sobolev, O. S., "Odnotipnyye svyazannyye sistemy regulirovaniya" [Coupled Regulation Systems of the Same Type], Moscow, 1973.

70. Besekerskiy, V. A. and Ye. P. Popov, "Teoriya sistem avtomaticheskogo regulirovaniya" [Theory of Automatic Control Systems], Moscow, 1966.

71. Severov, L. A., "Synthesizing the Parameters of a One-Axis Gyrostabilizer on an Integrating Gyroscope With Typical Intermittent Perturbation," TRUDY LIAP, No 49, 1966.

72. Formal'skiy, A. M., "Upravlyayemost' i ustoychivost' sistem s ogranichennymi resursami" [The Controllability and Stability of Systems With Limited Resources], Moscow, 1974.

73. Popov, Y. M., "New Criterion of the Stability of Nonlinear Automatic Systems," REV. D'ELECTR. ET D'ENERG., No 1, 1960.

74. Juri, E. and B. Lee, "Absolute Stability of Systems With Many Nonlinearities" AVTOMATIKA I TELEMEKHANIKA, No 6, 1965.

75. Juri, E. and B. Lee, "Theory of the Stability of Automatic Systems with Many Nonlinearities," in "Trudy-3-go Mezhdunarodnogo kongressa IFAK" [Proceedings of the Third International Conference of IFAC], Moscow, 1971.

76. Yakubovich, V. A., "Frequency Conditions of the Absolute Stability of Control Systems With Several Nonlinear or Linear Transient Blocks," AVTOMATIKA I TELEMEKHANIKA, No 6, 1967.

77. "Metody issledovaniya nelineynykh sistem avtomaticheskogo upravleniya" [Methods of Investigating Nonlinear Automatic Control Systems] edited by R. A. Nelepik, Moscow, 1975.

78. Popov, V. M., "The Absolute Stability of Nonlinear Automatic Control Systems," AVTOMATIKA I TELEMEKHANIKA, No 8, 1961.

79. Ayzerman, M. A. and F. R. Gantmakher, "Absolyutnaya ustoychivost' reguliruyemykh sistem" [The Absolute Stability of Regulated Systems], Moscow, 1963.

80. Naumov, B. N., "Teoriya nelineynykh avtomaticheskikh sistem" [The Theory of Nonlinear Automatic Systems], Moscow, 1972.

CONTENTS

6521
CSO: 1862

UDC 621.373:826.038.823

A FLASHLAMP PUMPED IODINE LASER WITH AN OPTICALLY THICK MEDIUM

Moscow KVANTOVAYA ELEKTRONIKA in Russian Vol 7, No 5, May 80 pp 944-952
manuscript received 4 Jul 79

[Paper by G.N. Vinokurov, V.Yu. Zalesskiy and P.I. Krepostnov]

[Text] A procedure for and some results of numerical calculations of the timewise and radial functions of the power and energy of laser radiation are described in this paper as applied to a photodissociative CF_3I iodine laser, as well as the index of refraction for the free lasing and inversion storage modes in the case of cylindrical symmetry of the pumping source, which is located directly in the gaseous active medium of the laser. The laser characteristics are analyzed as a function of the working gas pressure, the degree of dilution, the flashlamp radius, the resonator loss factor as well as the waveform and width of the pumping pulse.

It is advantageous to arrange the pump flashlamp directly in the active medium of a laser having large transverse dimensions so as to reduce pumping photon losses. Such a case is studied in this paper as applied to a photodissociative iodine laser using iodine trifluoromethane.

In contrast to paper [1], where the characteristics of a laser with a plane separation boundary between the pumping source and the active medium were calculated, this paper deals primarily with the case where the luminous surface is the side surface of a cylinder of radius ρ, while the active medium is bounded from within by a coaxial surface with a somewhat greater radius ρ'. The gap between these surfaces, having a thickness of $\rho' - \rho$ is transparent in the region of the spectrum used for the pumping. This case is amenable to an experimental check, and we hope that the comparison of the calculated and experimental characteristics will either confirm or assist in improving the accuracy of the existing concepts of the photochemistry of an iodine laser.

The investigation was based on numerical calculations of the timewise and radial functions of the energy and power of the laser pulse, the temperature,

density, velocity and pressure of the gas, the concentrations of the molecules of the working substance, the buffer gas and the photolysis products in accordance with a program compiled taking into account the latest data on elementary processes, which are coordinated with the data of laser experiments in the case of an optically fine active medium.

The transition to a description of an optically thick medium is made, just as in [1], taking into account the thermal deformation of the contours of the CF_3I and I_2 absorption bands. The angular distribution of the radiation of the cylindrically shaped pumping source is taken into account by numerical integration with respect to two angles (ϕ and θ) and integration over the spectrum in a range of 180 to 700 nm (23 frequency intervals). Also taken into account in the framework of the adopted model were the photochemical and relaxation chemical processes, as well as the gas dynamics of an inhomogeneously heated gas.

The calculations were performed using the procedure described in [1], with the following changes:

1. The terms with spatial derivatives of the $\partial(un_i)/\partial x$ type in equations (1)--(9) of paper [1] are replaced by the expressions $([1/r] + \partial/\partial r)un_i$ in accordance with the axial symmetry of the pumping source where a cylindrical system of coordinates is used (it is easy to confirm that equation (12) in [1] remains in force).

It is appropriate to note here that the term $N_A^{-1}\sum_{i=2}^{i=8}\frac{\partial n_i}{\partial t}\varepsilon_i$, was omitted in the right side of equation (9) in [1], where this term takes into account the change in the internal energy of the gas when its chemical composition changes, although this term was actually taken into account in the numerical calculations in [1] (N_A is Avogadro's number; ε_i is the internal energy of the microparticle field of the i-th kind; $\partial n_i/\partial t$ is the rate of change of the concentration of these microparticles due to the chemical processes).

2. The following formula was used to compute the internal energy ε_i instead of expression (24) in [1], which contains an error in the logarithmic term:

$$\varepsilon_i = N_A^{-1}\sum_{i=2}^{i=8} n_i\{e_i(T_0) + [(C_0)_i + (C_1)_i/(C_2)_i](T-T_0) - [(C_1)_i/(C_2)_i^2]\times$$
$$\times \ln[1 + (C_2)_i(T-T_0)]\}.$$

3. In accordance with the cylindrical shape of the pumping source, the following expressions were used for the probability of pumping radiation photon absorption, γ_j, and the optical density D:

$$\gamma_j = 8c \int_{k_1}^{k_2} \frac{k^3 \sigma_j(k, \mathcal{R})\, dk}{\exp\left(\frac{hc}{k_B} \frac{k}{T_{\text{ист}}}\right) - 1} \int_0^{\varphi_0(\rho, \mathcal{R})} d\varphi \int_0^{\pi/2} d\theta \times$$

$$\times \frac{\cos\theta \rho^2 (\mathcal{R}\cos\varphi - \rho) \exp(-D)}{(\mathcal{R}^2 \cos^2\theta + \rho^2 - 2\rho\mathcal{R}\cos\varphi\cos^2\theta)^{3/2}}, \quad (1)$$

$$D = \frac{1}{\cos\theta} \int_{\rho'}^{\mathcal{R}} dr\, (\sigma_1 n_1 + \sigma_9 n_9 - \sigma_{13} n_6) \times$$

$$\times \sqrt{\frac{\mathcal{R}^2 \cos^2\theta + \rho^2 - 2\mathcal{R}\rho\cos\varphi\cos^2\theta}{\mathcal{R}^2 + \rho^2 - 2\mathcal{R}\rho\cos\varphi - \rho^2\mathcal{R}^2\sin^2\varphi/r^2}}, \quad (2)$$

which differ from expressions (25) and (26) respectively, given in [1]. The subscript j for γ_j and σ_j indicates the number of the process (see below) in which pumping photon absorption occurs. σ_j is the absorption cross-section, which depends on the wave number k. Because of the inhomogeneous spatial distribution of the temperature and the function σ_j (T), σ_j also depends on the coordinates of the observation point. Other symbols are: c is the speed of light; k_B is Boltzman's constant; h is Planck's constant; the designations of the coordinates are clear from Figure 1, in which the elements of the radiating surface (point A) and the volume of the active medium for which the calculation is made (point M) are depicted in two orthogonal projections. The point M' lies on the path of the light beam from A to M. Its coordinates, expressed as functions of the angles θ and ϕ are used in the calculation of D. B is the point of contact of the tangent drawn from M to the surface of the cylinder falling in the plane perpendicular to the axis of the cylinder and passing through the point M. In this case, OM = R; O'M' = r; O"A = ρ; the angles are AOA" = = θ, A"OM = ϕ and BOM = ϕ_0. The numeration of the processes, j and the kinds of microparticles, i, are the same as in [1]:

1. $RJ + h\nu \longrightarrow R + \begin{cases} J^*J^*, \\ fJ \end{cases}$
2. $J^* + R \rightarrow RJ$,
3. $J^* + M \rightarrow J + M$,
4. $J^* + J_2 \rightarrow J + J_2$,
5. $2J + M \rightleftarrows J_2 + M$,
6. $2J + RJ \rightleftarrows J_2 + RJ$,
7. $2J + J_2 \rightleftarrows 2J_2$,
8. $RJ \rightleftarrows R + J$,
9. $J_2 + h\nu \rightarrow 2J$,
10. $2R \rightarrow R_2$,
11. $R + J_2 \rightleftarrows RJ + J$,
12. $R + RJ \rightarrow RF + R' + J$,
13. $R' + h\nu \rightarrow (R')^* \rightarrow R'$.

[J = Iodine]

It should be noted that an error was made in equation (25) in [1]. To obtain the correct values of γ_j, $\sin\theta$ in it should be replaced by $(1/2)\sin 2\theta$. Because of the errors noted and the more precise specification of the constants (see below), a number of variants of the "plane" problem were computed anew. Some of the results are given below and are compared

with the data of [1]. The numerical calculations, just as in [1], were performed for the case where the radical R is CF_3, while the buffer gas is the SF_6 molecules. The other symbols are: R' is CF_2, J* [= I*] is $J(5^2P_1/2)$, J[= I] is $J(5^2P_3/2)$, F is a fluorine atom, f* and f are the quantum efficiencies of the atoms averaged over the spectrum (the RI, I_2 and ZF_2 absorption bands which fall in the frequency range being studied are taken into account). The concentrations of these microparticles are: [RI] = n_4, [I_2] = n_3 and [CF_2] = n_6. Just as in [1], it is assumed that the CF_2 radicals absorb in a narrow frequency range ($\Delta k \approx 300$ cm^{-1}) in the region of $k \approx 4 \cdot 10^4$ cm^{-1} and shield only a small portion of the CF3I absorption band. However, this question requires further study because of the possible widening of the CF_2 absorption region with a rise in temperature.

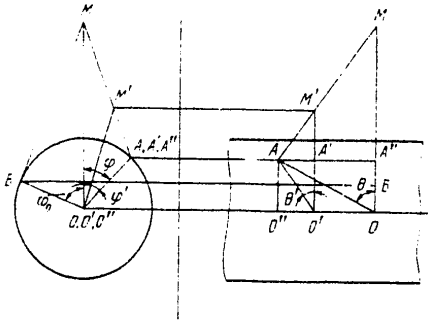

Figure 1. The elements of the radiating surface in two orthogonal projections.

More precise values than found in [1] were used for a number of constants. Because of paper [2], the values of the rate and thermal effect constants for processes 8 and 11 were specified somewhat more precisely. Other less important constants were also made more precise. The value of A_7 was corrected: the pre-exponential function in the Arrhenius expression for the rate constant of process 7: $K_7=A_7 \cdot \exp(-T_7/T)$ (in [1], twice the value of A_7 was used erroneously). All of the more precise constants are shown in Table 1.

Just as in paper [1], we neglect the influence of the weak compression wave arising because of the vaporization of the gas adsorbed by the walls of the laser chamber. It can be hoped [3] that this harmful influence will be successfully eliminated.

The initial and boundary conditions for the calculated variants and the results of computing the energy in the laser pulse, referenced to 1 cm^2

of the side surface of the pumping source are shown in Table 2 (all of the data applied to pumping pulses 100 microseconds wide).

TABLE 1

Constant	Adopted Value	Remarks
H_1, Kcal/mole	34.9	The yield of unexcited iodine atoms is taken into account
A_5, cm^6/sec	$1.8 \cdot 10^{-33}$	An improvement in the precision of the data which was used in [1]
T_5, °K	-1,050	
A_7, $°K^{-3/2} \cdot cm^6/sec$	$6.15 \cdot 10^{-38}$	
A_8, sec^{-1}	$4.3 \cdot 10^{16}$	The data from self-consistent processing of the previous experimental results [2]
T_8, °K	$2.6 \cdot 10^4$	
H_8, Kcal/mole	-52.8	
K_{11}, cm^3/sec	$1.6 \cdot 10^{-12}$	
A_{-11}, cm^3/sec	$4.6 \cdot 10^{-11}$	
T_{-11}, °K	8,400	
H_{11}, Kcal/mole	16.8	
H_{12}, Kcal/mole	18.2	An estimate taking into account the data for other halogens

We shall treat only those results which are important for an understanding of the energy characteristics of the laser. The radial distribution of the free lasing power for various points in time is shown in Figure 2.

As can be seen from Figure 2a, in the case of relatively slight dilution of the working gas with the buffer ($d = [SF_6]/[CF_3I] = 2$) when $\rho = \infty$ (a plane unbounded pumping source with constant brightness), there occurs almost uniform motion of the lasing region with a slight retardation.

For a cylindrical source with $\rho = 0.75$ cm, the radial functions of the specific power w are shown in Figure 2a (curves 6 and 7) as well as the distribution $w' = wR/\rho$ (curves 8 and 9), which describe the specific power referenced to a unit area of the pumping source. The quantity w' should be compared with the specific laser radition power of a plane pumping source, w_{pl}, since in this case, it turns out to be referenced immediately because $R/\rho = 1$ and $w'_{pl} = w_{pl}$. A comparison of w_{pl} and w' for a cylindrical source shows that in this case, the motion of the lasing zone is much more weakly expressed and is retarded very rapidly.

TABLE 2

(1) (2) (3) (4) (5) (6) (7) Таблица 2

(1) Номер опыта	(2) Максимальная яркостная температура, 10^3 K	(3) Давление CF_3J, мм рт. ст.	(4) Степень разбавления	(5) Радиус источника, см	(6) Энергия с 1 $см^2$ источника накачки*), Дж/$см^2$	(7) Коэффициент потерь, $см^{-1}$	(8) Форма импульса накачки
1	15	20	1,25	0,75	0,463	0,01	Параболическая (9)
2	15	20	2,5	0,75	0,463	0,01	То же
3	15	20	5	0,75	0,408	0,01	То же
4	15	10	2,5	0,75	0,344	0,01	То же
5	15	30	2,5	0,75	0,491	0,01	То же The same
6	15	40	2,5	0,75	0,498	0,01	То же
7	15	60	2,5	0,75	0,463	0,01	То же
8	12	20	2	0,75	0,275	0,01	Прямоугольная (10)
9	12	20	2	0,75	0,226	∞	То же
10	12	20	2	∞	0,334	0,01	То же
11	12	20	2	∞	0,270	∞	То же
12	12	20	5	∞	0,320	0,01	То же The same
13	12	20	5	∞	0,260	∞	То же
14	13,5	20	2,5	0,75	0,456	0,01	То же
15	15	10	2,5	0,75	0,240	0,033	Параболическая (9)
16	15	10	2,5	∞	0,380	0,033	То же
17	15	20	2,5	0,75	0,310	0,033	То же The same
18	15	20	2,5	∞	0,390	0,033	То же

*The stored energy, which is defined as $(2/3)h\nu N$, where $(2/3)h\nu = 1.0 \cdot 10^{-19}$ J is given for the storage mode (a loss factor of ∞).

Key: 1. Number of the trial;
2. Maximum brightness temperature, 10^3 °K;
3. CF_3J pressure, mm Hg;
4. Degree of dilution;
5. Radius of the source, cm;
6. Energy from 1 cm^2 of pumping source*, J/cm^2;
7. Loss factor, cm^{-1};
8. Waveform of the pumping pulse;
9. Parabolic;
10. Rectangular;

In the case of considerable dilution (d = 5), in the case of any real pumping source where $T_{real} \simeq 1.2 \cdot 10^4$ °K and a pulse width of Δt_H [$=t_{pump}$] < $< 10^{-4}$ sec, the motion of the lasing region can be disregarded (see Figure 2a, curves 4 and 5). It can be seen from Figure 2b how the lasing region changes in case of higher power pumping with a parabolic waveform pulse, which was described by the expression $I(t) = I_{max}4t(1 - t/\Delta t_H)/\Delta t_H$, where Δt_H is the pulse width, which was taken as equal to 100 microseconds;

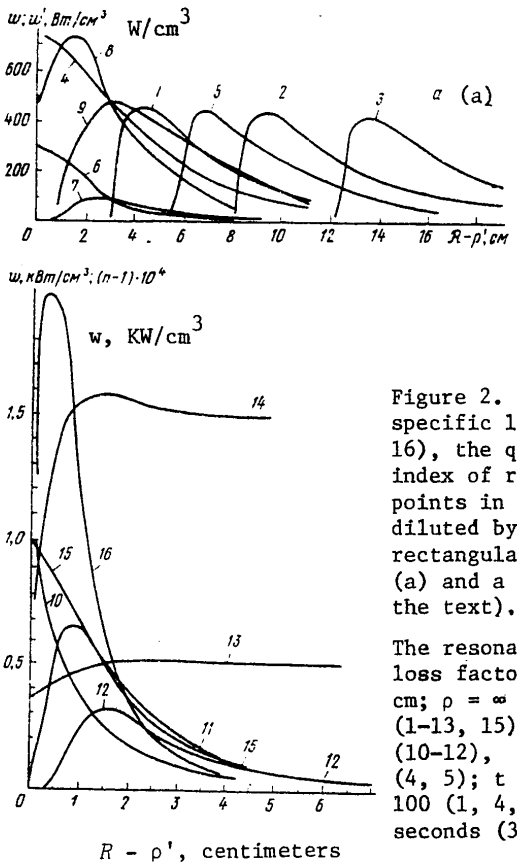

Figure 2. The radial distribution of the specific laser power $w(R)$ (1-7, 10-12, 15, 16), the quantity $w' = wR/\rho$ (8, 9) and the index of refraction n (13, 14) for various points in time t in the case of CF_3I, diluted by the elemental gas SF_6, for a rectangular pulse with T_{real} = 12,000 °K (a) and a parabolic pumping pulse (b) (see the text).

The resonator losses were determined by the loss factor K_{loss} = 0.01 cm^{-1}, $\rho' - \rho$ = 0.25 cm; $\rho = \infty$ (1-5) and 0.75 cm (6-16); p_{RI} = 20 (1-13, 15) and 60 mm Hg (14, 16); d = 1.25 (10-12), 2 (1-3, 6-9), 2.5 (13-16) and 5 (4, 5); t = 20 (10), 60 (11, 13-16), 80 (12), 100 (1, 4, 6, 8), 200 (2) and 300 microseconds (3, 5, 7, 9).

I_{max} is the pumping photon flux density in the center of the first (working) absorption band at the maximum of the pumping pulse $t_{max} = \Delta t_H/2$. It was computed from the specified values of T_{real} assuming a Planck spectral distribution. As was established by the calculation, the "tail" of actual pumping pulses, which is not taken into account in calculations with parabolic pulses, has practically no influence on the energy characteristics of the laser.

It likewise follows from the calculations that the distribution of the lasing energy with respect to the radius during the time of a pumping pulse and the total energy practically do not depend on the waveform of this pulse (rectangular and parabolic pulses were compared for the case of almost identical energy radiated over the pumping time, see Table 2, trials 2 and 14).

Knowing the radial functions of the concentrations of the gases and by estimating their molecular refractions from data found in the literature, one can compute the profile for the index of refraction in the active medium. The index of refraction of the active medium is shown in Figure 2b as a function of R for λ = 1,315 nm. It can be seen that the gradient of the index of refraction, ∇n, is especially high close to the source, at a distance of up to about 1 cm from it.($R \approx 1.75$ cm). At an iodide pressure of p_{RI} = 60 mm Hg and d = 2.5, in a range of $R \approx$ ≈ 1-1.5 cm, $\nabla \approx 7 \cdot 10^{-5}$ cm^{-1}, and at a pressure of 20 mm Hg and d = 2.5, $\nabla n \approx 10^{-5}$ cm^{-1}. At a greater distance, ∇n becomes small, while the active medium is optically completely homogeneous. From the viewpoint of optical homogeneity, an iodide pressure of $\leq$ 20 mm Hg is preferable (d = 2.5), since only in this case does the region of elevated values of ∇n take in the portion of the lasting zone which makes a small contribution to the total (with respect to the cross-section) laser radiation power.

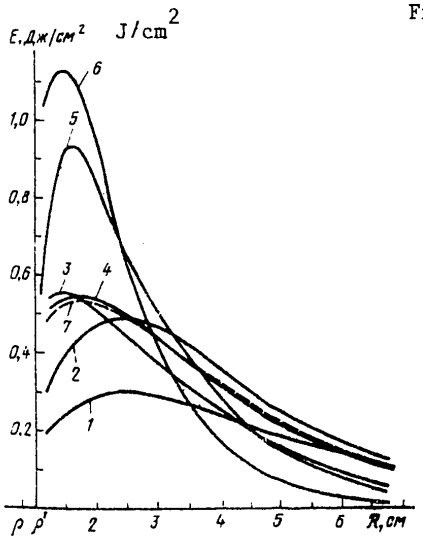

Figure 3. The radial distributions of the specific energy in a laser pulse $E(R)$ multiplied by $2\pi R$, at the maximum of a parabolic pumping pulse where T_{real} = 15,000 °K.

Key: ρ = 0.75 cm; K_{loss} = = 0.01 cm^{-1}; p_{RI} = 10 (1), 20 (2-4), 40 (5) and 60 mm Hg (6); d = 1.25 (2), 2.5 (1, 4-6) and 5 (3); curve 7 corresponds to a rectangular pumping pulse where T_{real} = = 13,500 °K with a width of 100 microseconds where p_{RI} = 20 mm Hg and d = 2.5.

It can be seen from Figure 3 that in the case of dilutions close to the optimal with respect to the total laser energy efficiency, $E_{\text{п}} = \int_{\rho'}^{\mathcal{R}} E(\mathcal{R}) 2\pi \mathcal{R} d\mathcal{R}$, a marked widening of the energy extraction region should be observed with a decrease in d in the case of a weak dependence of $E_{\text{п}}$ on (d) (d ≈ 1-5). As follows from Figure 2, this widening is a

consequence of the movement of the lasing region, which becomes faster the smaller d is.

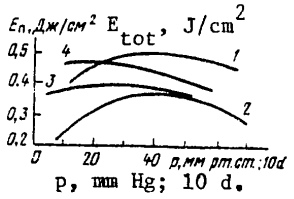

Figure 4. The laser pulse energy, referenced per cm^2 of surface of the pumping source, as a function of p_{RI} where d = 2.5 (1-3) and as a function of d where p_{RI} = 20 mm Hg (4) at the maximum of a parabolic pulse with T_{real} = 15,000 °K.

ρ = 0.75 cm (1, 2, 4) and ∞ (3); K_{loss} = 0.01 (1) and 0.033 cm^{-1} (2-4).

The widening of the energy extraction region in a radial direction, which arises because of a drop in the partial pressure of the working gas, is simply a consequence of the fact that the photon path length is an inverse function of the working gas pressure p_{RI}. As has already been indicated, in the case of a low working gas pressure, the active medium is more homogeneous and is characterized by a small gradient n of the laser radiation and a correspondingly small beam divergence.

The total energy of a laser pulse is shown in Figure 4 as a function of p_{RI} in the case of a constant value of d = 2.5 and T_{real} = 15,000 °K (a parabolic pulse). In the case of ρ = ∞, the function $E_п$ (p_{RI}) is hardly noticeable and is characterized by a poorly expressed maximum at p_{RI} = = 20 mm Hg. This is not surprising if one considers the fact that in an unbounded active medium, the pumping radiation is totally absorbed, regardless of the pressure.

The drop in $E_п$ with a reduction in p_{RI} in the range $p_{RI} < p_{RI}^{max}$ is explained basically by the fact that the inverse recombination process does not have time to cope with the clearing of the lower lasing level. In this case, the lasing is accompanied by an increase in the concentration of I and I* atoms, while the energy of the laser pulse falls off and can approach the value $g_2/(g_1 + g_2) = 2/3$ of the maximum value of $E_п$ (in the case of poor clearing of the lower level) (g_1 and g_2 are the statistical weights of the I* and I levels).

The pyrolysis process (J = 8) has no direct influence on the laser pulse energy, and leads only to a shifting of the lasing region. It can be manifest indirectly in an increase over time of the thickness of the layer affected by the pyrolysis, which can contain absorbing products of the CF_2 type. However, with an increase in p_{RI} with constant values of d, Δt_H and T_{real}, the optical density of these products likewise remains approximately constant.

The decrease in E_π with an increase in p_{RI} when $p_{RI} > p_{RI}^{max}$ is explained by the increase in the contribution of the extinguishing of I* by iodine molecules (j = 4) because of the fact the rate of their formation in the j = 6 process, $v_6 = k_6 [I]^2[RI]$ (just as v_5) is proportional to p_{RI}^m, where $m \geq 2$, while the pumping rate γ_1 is proportional to p_{RI}.

When ρ = 0.75 cm (see Figure 4, curves 1 and 2), the functions E_π (p_{RI}) have a more sharply pronounced maximum (the values of $E_\pi/2\pi\rho$ are given in Figure 4 for convenience in making the comparison with $\rho = \infty$). The steeper drop when $p_{RI} < p_{RI}^{max}$, which occurs in this case, and the shift of p_{RI}^{max} in the direction of an increase (as compared to $\rho = \infty$) are explained by the increase in the percentage of the pumping photons η_H, which are absorbed in the region where the lasing threshold is not reached. This result is a consequence of the weakening of the pumping with an increase in R when $\rho < \infty$ (just as $1/R$ when $\rho << R$). Even in the absence of a pumping medium which absorbs photons.

The critical role of the factor η_H [= $\eta_{pumping}$] is confirmed by the comparison of curves 1 and 2 in Figure 4 which were attained for conditions which differ only in the resonator losses. The loss coefficient K_{loss} is equal to 0.01 cm^{-1} for curve 1 and 0.033 cm^{-1} for curves 2 and 3, while the length of the active medium is equal to 1 m. In the region of total pressures t on the order of 10 mm Hg and below, the drop of Figure 2 should become even greater because of the increase in the contribution of doppler widening of the line which does not depend on p. The applies to a considerable extent to curve 3 also.

The reduction E_π with the rise in p_{RI} when $p_{RI} > p_{RI}^{max}$ in the case where $\rho < \infty$ is due to the same factors as for the case of $\rho = \infty$. For this reason, in the range of large values of p_{RI}, where the pumping photon path lengths become small as compared to ρ, the difference between the cases where ρ = 0.75 cm and $\rho = \infty$ becomes insignificant. By comparing curves 2 and 3 in Figure 4, it can be concluded that this is what actually occurs.

Also shown in Figure 4 for p_{RI} = 20 mm Hg, ρ = 0.75 cm and K_{loss} = 0.01 cm^{-1} is the curve for E_π as a function of the degree of dilution with the buffer gas. It shows that for an unbounded medium, the degree of dilution of the iodine by the buffer gas has a slight influence on the quantity E_π. The dilution is useful in this case because it permits a significant reduction in the volume handled by the pumping (see Figure 2) and correspondingly, in the transverse dimensions of the laser chamber. Moreover, the danger of shielding by absorbing photolysis products is reduced, something which has not yet been adequately studied.

In contrast to the free lasing mode, it is not the lasing region which is shifted during operation in the storage mode ($K_{loss} = \infty$), but rather the stored population inversion region which contains the excited iodine

atoms. It is important to note that with steady-state motion of this region, pumping does not perform any useful work, since the rate of formation of I* atoms is equal to the rate of their destruction close to the rear boundary of this region due to their interaction with the heated and extinguishing products of photolysis and pyrolysis. In order for the efficiency not to be too low, the gating time, $\Delta t_{turn-on}$, should not be too large, while the degree of dilution d should not be too low. The optimal values of d are significantly higher than in the case of free lasing (see [1]).

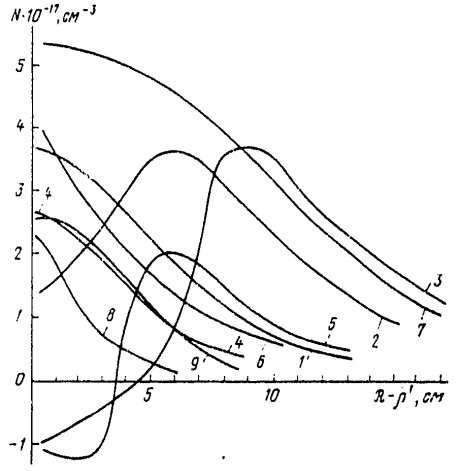

Figure 5. The radial distributions of the stored population inversion N (storage mode) in the case of a rectangular pulse with T_{real} = 12,000 °K and p_{RI} = 20 mm Hg.

$\rho' - \rho$ = 0.25 cm; $\rho = \infty$ (1-7) and 0.75 cm (8, 9); d = 2 (1-5, 8, 9) and 5 (6, 7); t = 100 (1, 4, 6, 8), 200 (2), 260 (5) and 300 microseconds (3, 7, 9).

The radial distributions of the population inversion at various points in time are shown in Figure 5 for p_{RI} = 20 mm Hg and a rectangular pumping pulse with T_{real} = 12,000 °K (d = 2). Curves 1 - 3 illustrate the motion of the region of stored energy when $\rho = \infty$. It can be seen from a comparison of them and the curves 6 and 7 that the dilution of the SF_6 down to a value of d = 5 where $\Delta t_{turn-on}$ = 300 microseconds makes it possible to store significantly more energy. Curves 4 and 5 were taken from [1] and show that the innaccuracies allowed in [1] markedly understate the values of the stored energy. Curves 8 and 9 apply to the case

apply to the case where $\rho = 0.75$ cm. In order to compare the energies removed per unit surface of the pumping source for $\rho = 0.75$ cm and $\rho = \infty$, the inversion of the populations should be multiplied by the ratio R/ρ in the first case.

Data on the total (integrated over the cross-section) laser power in the free lasing mode (Figure 6a) and for the stored energy (for the storage mode) are compared in Figure 6 as a function of time d = 2 and 5 and $\rho = 0.75$ cm and ∞. It can be seen from a comparison of curves 2 and 3 that when $\rho = \infty$, for short pumping pulses ($\leq$ 60 microseconds when T = = 12,000 °K), a higher energy in a pulse is achieved when d = 2. However, the case where d = 2 is all the same less favorable, even for the case of a short pumping pulse since a greater depth in the working of the active medium is required for its realization. When $\rho = 0.75$ cm, the power is lower than for any values of t.

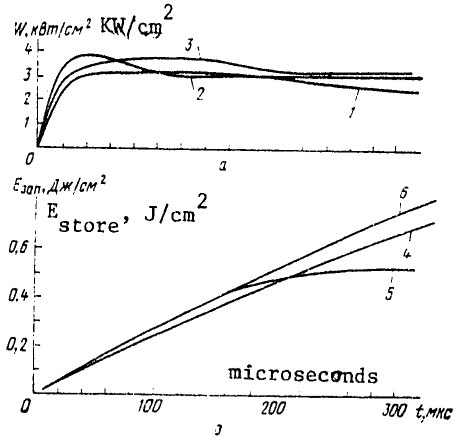

Figure 6. The timewise curves for the total power W in the free lasing mode (K_{loss} = 0.01 cm^{-1}) (a) and the stored energy, E_{store}, in the storage mode (b) when pumped by a rectangular pulse where T_{real} = 12,000 °K at p_{RI} = = 2.0 mm Hg.

The values of W and E_{store} are referenced to 1 cm^2 of surface of the pumping source; $\rho = 0.75$ cm (1, 4) and ∞ (2, 3, 5, 6); d = 2 (1, 2, 4, 5) and 5 (3, 6).

A clearer advantage of considerable dilution is manifest in the storage mode (Figure 6b). In this case, a single cylindrical flashlamp at the maximum yields an energy per unit of luminous surface which is greater, the smaller its radius is. It is apparent that the most favorable arrangement is that where the pumping lamps are positioned in the active medium, in which the volume of the active medium region is minimal where the absorption of pumping photons does not lead to the lasing threshold being exceeded or leads to lasing only at the end of a pumping pulse.

Main Conclusions

1. When cylindrical excitation flashlamps are placed directly in the active medium, the gradient of the index of refraction in the region contiguous with the lamps, where this gradient arises primarily because of gas heating and motion, can reach 10^{-5} to 10^{-4} cm^{-1} in the case of SF_6 dilution where $d \approx 2.5$. In this case, with a rise in the initial CF_3I pressure from 20 to 60 mm Hg, the percentage of laser radiation energy falling in the region of strong inhomogeneity is substantially increased.

2. The total laser radiation energy in a free lasing pulse depends slightly on the degree of dilution with the buffer gas (in contrast to the case of an optically fine medium). With an increase in d, it falls off slowly because of the increase in the threshold inversion, and consequently, in the fraction of pumping photons adsorbed in the active medium region where the lasing threshold is not reached. With an increase in d, the diameter of the lasing decreases substantially.

3. The total energy as a function of the working gas pressure with a constant value of d has a maximum (in contrast to the case of an optically fine medium), which is narrower, the smaller the radius of the pumping source.

BIBLIOGRAPHY

1. G.N. Vinokurov, V.Yu. Zalesskiy, KVANTOVAYA ELEKTRONIKA [QUANTUM ELECTRONICS], 5, 2110 (1978).

2. V.Yu. Zalesskiy, A.M. Kokushkin, KINETIKA I KATALIZ [KINETICS AND CATALYSIS], 21, No 2, 552 (1980).

3. K. Hohla, SPRINGER SER. OPT. SCI., 9, 139 (1978).

8225
CSO: 1862

UDC 621.375.8

THE PLASMA PARAMETERS IN DISCHARGE AFTERGLOW IN A COPPER VAPOR LASER

Moscow KVANTOVAYA ELEKTRONIKA in Russian Vol 7, No 5, May 80 pp 988-992
manuscript received 6 Sep 79

[Paper by V.M. Batenin, I.I. Klimovskiy, M.A. Lesnoy and L.A. Selezneva, High Temperature Institute of the USSR Academy of Sciences, Moscow]

[Text] The electron concentration and temperature and electron distribution over the radius of the discharge tube were measured and the degree of ionization of the copper atoms along the discharge axis was estimated in the discharge afterglow in a copper vapor laser, operating in a periodic pulsed mode at a frequency of f ≈ 7 KHz.

A little studied form of a high voltage (electrical field intensity on the order of 100 v/cm), pulsed (voltage pulse width of from tens to hundreds of nanoseconds) and periodic (voltage pulse repetition rate of up to 100 KHz) discharge in a mixture of an inert gas and a metal vapor is realized in spontaneous heating lasers using metal vapors [1]. Ionization, excitation of the active medium and lasing occur during the voltage pulses, while relaxation of the plasma and restoration of the initial parameters of the active medium occur between the pulses. It is apparent that for the direct understanding of the processes taking place in the active medium and which determine both the power of the lasing pulses and their maximum repetition rate, it is necessary first of all to know the timewise changing parameters of the plasma.

The electron concentration n_e and the gas temperature T_g in a copper vapor laser were pre iously measured by the authors of this paper [2, 3]. Primary attention is devoted in this paper to a study of such parameters of the relaxing plasma as the concentration and temperature of the electrons, the distribution of the concentration and temperature of the electrons over the radius of the discharge tube and others under the same conditions under which the gas temperature measurements were made previously.

TABLE

Buffer Gas Буферный газ	Давление, (1) кПа	T_g (0), °K	T_e к, K	$T_{e\,ср}$, K °K avg
Неон Neon	13,5	4500	2900	4250±300
Неон Neon	3,3	4200	2500	4900±350
Гелий Helium	3,3	4000	4000	4200±200
Аргон Argon	2,9	4200	2800	4300±500

Key: 1. Pressure, KPa.

The laser described earlier in [3], with a dishcarge tube 70 cm long and 1.2 cm in diameter served as the object of study. Helium, neon and argon were used as the buffer gases. The excitation of the discharge was accomplished using a circuit with resonant charge exchange of a storage capacitor which is described in [3]. The energy contribution to the discharge during the voltage pulse amounted to about 2 mJ/cm^3. The pressure of the buffer gases varied in a range of from 1.8 to 13.3 KPa. The power consumed from the power source was maintained in all experiments at the same level of W_{supply} = 2 KW. Depending on the kind and pressure of the buffer gas, the excitation pulse repetition rate varied in a range of from 6.5 to 8 KHz.

One of the main parameters of the plasma in a copper vapor laser is the gas temperature. Values of the gas temperature T_g (0) on the axis of the discharge tube for various buffer gases are given in the table. The values of T_g (0) for neon were borrowed from [3], while those for helium were computed from the doppler widening of the 318.77 nm helium line, measured by means of an IT28-30 interferometer, crossed with an ISP-30 spectrograph. For more details on the measurement procedure, see [3]. The temperature T_g (0) was not measured for argon, however, appropriate estimates showed that it is no lower than for neon. For this reason, the value of T_g (0) in neon is given as an approximate value of the temperature of the heavy particles in argon.

The concentration of electrons, which is one of the most important parameters of the plasma of a copper vapor laser, was measured in the region of the discharge near the axis having a diameter of 2 to 3 mm by means of a dual beam laser interferometer, similar to that described in [2], at a wavelength of 10.6 micrometers. The measurement results are shown in Figures 1 and 2. By virtue of the fact that the timewise resolving power of the interferometer amounts to about 2 microseconds, the values of electron concentration at times less than 2 to 4 microseconds were reproduced by extrapolation of the time functions of n_e to the point in time t = 0, corresponding to the moment of completion of the pumping pulse.

The curves for the electron concentration at the point in time of concluding the pumping pulse $n_e\ (0)_{max}$ are shown in Figure 3 as a function of the kind and pressure of the buffer gas.

It is apparent that the restoration of the original properties of the active medium will take place in different ways depending on what percentage of the atoms are ionized in the process of exciting discharge. The degree of ionization of the copper atoms can be determined by comparing the maximum electron concentration $n_e\ (0)_{max}$ with the initial concentration of the copper atoms. Estimates made taking into account the temperature of the wall of the discharge tube ($T_{wall} \approx 1{,}500$ °C), which determines the copper vapor pressure [4] in the discharge, and the gas temperature along the axis of the discharge tube (see the table), yield a value for the concentration of the copper atoms on the axis of the discharge tube of $n_{Cu}\ (0) \approx 7 \cdot 10^{14}$ cm^{-3}. At low buffer gas pressures, this pressure will be somewhat reduced by virtue of the diffusion transport of the copper atoms through the end face of the discharge tube. A comparison of the functions plotted in Figure 3 with the value of $n_{Cu}\ (0)$ shows that at least in the region of the discharge tube near the axis the copper atoms are completely ionized during the time of the pumping pulse. The conclusion drawn here is rather important since if the copper atoms are completely or even to a significant extent ionized over the time of the pumping pulse, the restoration of the initial properties of the active medium will be determined by mechanisms different from those treated earlier by various authors (for example, see [5, 6]).

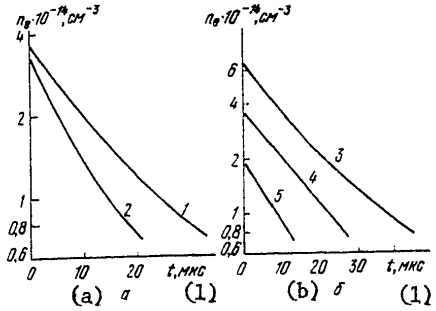

Figure 1. The electron concentration on the axis of the discharge tube as a function of time for argon at a pressure of 2.9 KPa (1); for helium at 3.3 KPa (2); for neon at 13.3 (3), 6.7 (4) and 3.3 KPa (5).

Key: 1. t, microseconds.

The electron temperature in the relaxing plasma can be determined from the functions for $n_e = f(t)$ [7]. However, before moving on to the

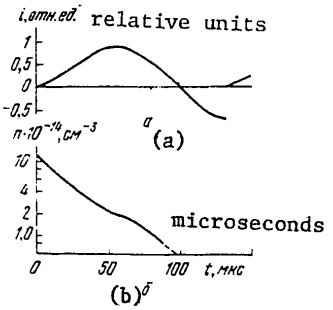

Figure 2. The charge exchange current (a) and electron concentration on the discharge tube axis (b) in argon as a function of time.

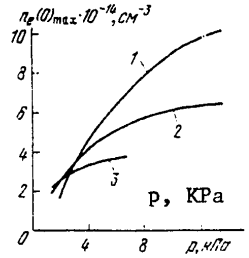

Figure 3. The electron concentration at the moment of completion of a pressure pulse as a function of buffer gas pressure for argon (1), neon (2) and helium (3).

determination of T_e from the functions shown in Figures 1 and 2, it is necessary to note that according to the data of paper [8], the level of the power introduced into the discharge in the period between pulses amounts to 150 watts, something which can have a substantial impact on the rate of relaxation of the concentration and temperature of the electrons. The correlation between the current flowing through the discharge and the relaxation rate of n_e in argon at a pressure of 13.3 KPa (see Figure 2) serves as a direct confirmation of the existence of this influence. A more detailed analysis has shown that in the interpulse period, the electrical energy is introduced into the discharge in a nonuniform manner; in the time interval which is of the greatest interest from the viewpoint of the restoration of the properties of the active medium (the first 30 microseconds), the energy contribution is small and cannot exert a substantial influence on the rate of the relaxation properties.

Since the electron concentrations, the timewise curves for which are shown in Figures 1 and 2, were measured in the discharge region near the axis, the following equation was used in calculating T_e:

$$\frac{\partial n_e(0)}{\partial t} = -\frac{6D_a}{r^2} n_e(0) - n_e(0)\left[\alpha n_e^2(0) - \beta n_{Cu}(0)\right], \qquad (1)$$

where n_e (0) and n_{Cu} (0) are the electron and copper atom concentrations respectively in the region of the discharge tube near the axis; r is the radius of the discharge tube; D_a, α and β are the ambipolar diffusion, the triple recombination and ionization coefficients respectively. We neglect the ionization of neon atoms, in accordance with the results of paper [2].

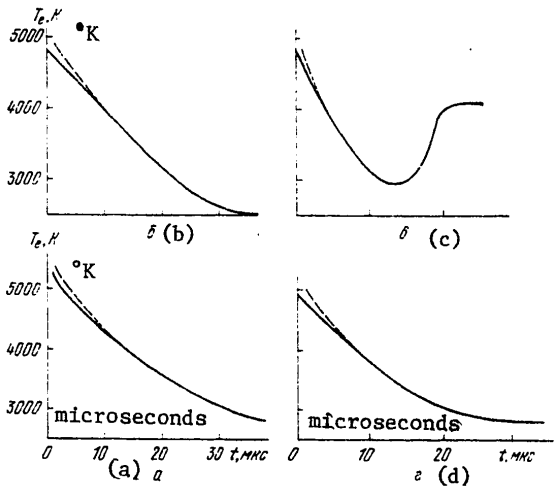

Figure 4. The electron temperature in the discharge afterglow as a function of time in the various buffer gases:

a. Neon, p = 13.3 KPa;
b. Neon, p = 3.3 KPa;
c. Helium, p = 3.3 KPa;
d. Argon, p = 2.9 KPa.

The ambipolar diffusion coefficient was computed assuming that the interaction of a copper ion with the atoms of the buffer gas is of a polarization nature [9]; α and β were computed in accordance with [10]. When computing D_a, the gas temperature was taken as 3,000 °K for neon and argon, and 2,500 °K for helium. The results of calculating the electron temperature in the relaxation period are shown in Figure 4 for a concentration of copper atoms of n_{Cu} (0) = 10^{15} cm^{-3}. Also shown there with the dashed line are the calculated values of the temperature assuming that n_{Cu} (0) = 0. It can be seen that 10 microseconds after the conclusion of the discharge, the electron temperature practically does not depend on the concentration of the copper atoms, and with the course of time, tends to a certain final value T_{eK} (see the table). For argon and neon, $T_{eK} < T_g$ (0); for helium, T_{eK} is close to T_g (0), something which is due to the heating of the electrons by the charge exchange current of the storage capacitance.

The distributions of the electron concentration and temperature averaged over time with respect to the cross-section of the dishcarge tube were

determined with respect to the intensity and frequency behavior of the recombination continuum in a range of wavelengths of 250 to 350 nm. The measurement of the CW intensity was made using a standard procedure [11] with the ISP-30 spectrograph. The radiation emitted from the center of the discharge tube through its end face was projected by means of the system of lenses onto the spectrograph slot. The radiation was recorded photographically. The anode crater of a carbon arc was employed as the calibration reference source of light.

The height of the spectrograph slot exceeded the diameter of the image of the discharge tube, something which made it possible to measure the temperature T_e and the relative concentration n_e/n_e (0) as a function of the tube radius.

An analysis of the continuous radiation in a spectral range of 250 to 350 nm showed that it has a decaying nature with a threshold in the 320 nm region. This radiation is equated to the photorecombination continuum at the $^2P_{1/2}$ and $^2T_{3/2}$ levels of a copper atom. Since in the plasma of the discharge studied here with buffer gases of neon, argon and helium there occurs predominantly ionization of the copper atoms, the continuous radiation during the photorecombination of the ions of the buffer gas was not taken into account.

The calculation of T_e and n_e was made using the relationship defining the intensity I_{ea} of the recombination continuum for frequencies exceeding the limiting frequency ν_g [12]:

$$I_{ea}(\nu) \sim \xi n_e^2 \exp\left[-h(\nu-\nu_g)/kT_e\right]/\sqrt{T_e}, \qquad (2)$$

where ξ is Biberman's factor; h and k are Planck's and Boltzman's constants respectively.

The estimates made using expression (2) taking into account the functions shown in Figures 1 and 2, showed that the plasma parameters measured with respect to the continuum correspond to the parameters in the first 10 to 20 microseconds following the conclusion of the pumping pulse.

The results of electron temperature measurements on the axis of the discharge tube, $T_e\ (0)_{avg}$, with respect to the drop in the continuum, are shown in the table. Within the limits of measurement error, satisfactory agreement is observed between the values of the temperature of the electrons reproduced based on the functions $n_e\ (0) = f(t)$ averaged over the first 20 microseconds and those measured with respect to the continuum. The measurement of the electron temperature in regions located at equal distances from the discharge tube axis showed that in all buffer gases, $T_{e\ avg}$ does not depend on the radius and $T_{e\ avg} = P_e\ (0)_{avg}$.

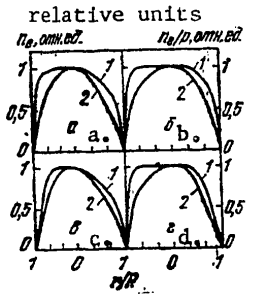

Figure 5. The distributions of the electron concentration (1) and n_e/p (2) with respect to the radius of the discharge tube for Ne, 13.3 (a) and 3.3 KPa (b); Ar, 3.3 KPa (c); He, 3.3 KPa (d).

The distribution of the relative electron concentration, n_e/n_e (0) was computed from the distribution of the continuum intensity with respect to the discharge radius at a fixed frequency ν. The results of the calculations for various buffer gases are shown in Figure 5. Also shown there are the quantities n_e/p which to a certain extent characterizes the plasma conductivity, as a function of the radius. Here p is the pressure of the buffer gas referenced to 0 °C; it was computed from the relationship:

$$p=p_0 273/T_g(r), \tag{3}$$

where p_0 is the total pressure of the buffer gas in the discharge tube; $P_g(r)$ is the gas temperature. The calculation of $T_g(r)$ was made with the assumption of a uniform distribution of the heat sources over the cross-section of the discharge tube:

$$T_g(r)=T_{ст}+\Delta T\ [1-(r/R)^2]. \tag{4}$$

The quantity T_{ct} was taken equal to 1,800 °K and ΔT was computed from the data of the table.

In analyzing the data shown in Figure 5, attention is drawn to the strong inhomogeneity and distortion of the discharge, leading to asymmetric distribution of the electron concentration and plasma conductivity over the cross-section of the discharge tube. The distortion of the dishcarge is primarily related to the interaction of the current flowing in the discharge and the supply wires, and can be eliminated by using coaxial structures for the current carrying components.

BIBLIOGRAPHY

1. G.G. Petrash, UFN [USPEKHI FIZICHESKIKH NAUK: PROGRESS IN THE PHYSICAL SCIENCES], 105, 645, (1971).

2. V.M. Batenin, V.A. Burmakin, P.A. Vokhmin, A.Ye. Yevtyunin, I.I. Klimovskiy, M.A. Lesnoy, L.A. Selezneva, KVANTOVAYA ELEKTRONIKA [QUANTUM ELECTRONICS], 4, 1572, (1977).

3. V.M. Batenin, V.A. Burmakin, P.A. Vokhmin, I.I. Klimovskiy, M.A. Lesnoy, L.A. Selezneva, [TEPLOFIZIKA VYSOKIKH TEMPERATUR], 16, 1145, (1978).

4. A.N. Zaydel', G.V. Ostrovskaya, Yu.I. Ostrovskiy, "Tekhnika i praktika spektroskopii" ["Spectroscopy Practice and Engineering"], Moscow, Nauka Publishers, 1976.

5. P.A. Bokhan, V.I. Solomonov, V.B. Shcheglov, KVANTOVAYA ELEKTRONIKA, 4, 1812, (1977).

6. V.Ye. Prokop'yev, V.M. Klimkin, IZV. VUZOV. SER. FIZIKA [PROCEEDINGS OF THE HIGHER EDUCATIONAL INSTITUTES. PHYSICS SERIES], 5, 152, (1978).

7. L.G. D'yachkov, G.A. Kobzev, ZHTF [JOURNAL OF ENGINEERING PHYSICS], 48, 2343, (1978).

8. I.I. Klimovskiy, L.A. Selezneva, TVT, 16, 27, (1978).

9. A.V. Yeletskiy, L.A. Palkina, B.M. Smirnov, "Yavleniya perenosa v slaboionizovannoy plazme" ["Transport Phenomena in a Weakly Ionized Plasma"], Moscow, Atomizdat Publishers, 1975.

10. L.M. Biberman, V.S. Vorob'yev, I.T. Yakubov, UFN [PROGRESS IN THE PHYSICAL SCIENCES], 107, 353, (1972).

11. "Metody issledovaniya plazmy" ["Methods of Studying a Plasma"], edited by V. Lokhte-Khol'greven, Moscow, Mir Publishers, 1971.

12. L.M. Biberman, G.E. Norman, UFN, 91, 193, (1967).

[165-8225]

8225
CSO: 1862

UDC 535.338.43+539.196.6+141.1+4+7

THE SPECTRAL DEPENDENCE OF THE ABSOLUTE QUANTUM YIELDS OF THE FORMATION OF $I(^2P_{1/2})$ AND $I(^2P_{3/2})$ ATOMS FOR THE CASE OF THE PHOTOLYSIS OF ORGANIC IODIDES: II. CF_3I, C_2F_5I, C_3F_7I, CF_3CFICF_3 AND $CF_3OCF_2CF_2I$

Moscow KVANTOVAYA ELEKTRONIKA in Russian Vol 7, No 5, May 80 pp 993-1005
manuscript received 18 Sep 79

[Paper by V.S. Ivanov, A.S. Kozlov, A.M. Pravilov and Ye.P. Smirnov, Scientific Research Institute for Physics at Leningrad University imeni A.A. Zhdanov]

[Text] A procedure for the measurement of the spectral functions of the absolute quantum yields of the formation of iodine atoms in the $^2P_{1/2}$ and $^2P_{3/2}$ states during photolysis of organic iodides, RI, is described and substantiated. Data obtained for RI = CF_3I, C_2F_5I, CF_3CFICF_3, C_3F_7I and $CF_3OCF_2CF_2I$ are cited and interpreted. The proposed model is checked by a calculation of the distribution of the electron density in RI.

Interest in the study of primary and secondary photolysis processes of alkyliodides and perfluoroalkyliodides (RI) has not abated despite the rather considerable time which has elapsed since creation of the first photodissociative iodine laser (FIL) by Kasper and Pimentel [1]. Moreover, while prior to 1975 quantitative experimental data were given in four papers in all [2-5] for the absolute quantum yields Φ_{I*} and Φ_J formations $I(^2P_{1/2})$ and $I(^2P_{3/2})$ respectively for RI photolysis at individual wavelengths, in recent years, the number of such papers has increased sharply [6-12]. However, a common drawback to many of them [6-10, 12] is the fact that in the given papers, the photodissociation was accomplished in a wide spectral range using integral light, and for this reason, for reasons discussed previously [13, 14] in the case where $\Phi_{I*}(\lambda) \neq 0$ or 1 throughout the entire photolysis spectral range, the results obtained are of value in the best case for radiation sources having the same spectra as in the papers cited here. In some experiments, photodissociation processes were studied at one absorbed quanta energy [2-5, 11, 12, 15].

Extremely more complete information on the mechanism and the processes of photodissociation (which can be used for any method of pumping in FIL's) and on the properties of the energy potential surfaces of the molecules at which there is a transition when a light quantum is absorbed, can be obtained when studying the spectral functions of the absolute quantum yields of the formation of the photodissociation products [13, 14]. This naturally, applies completely to the molecules discussed here. An understanding of the mechanism of RI photodissociation is necessary, in particular, so as to synthesize new working substances in a goal oriented manner for FIL's. Such information has already been presented in paper [14] for RI = C_3F_7I, CF_3CFICF_3 and $CF_3OCF_2CF_2I$. Data are given in this paper for the spectral functions $\Phi_{I*}(\lambda)$ and $\Phi_I(\lambda)$ in the 235-315 nm region for a broader group of objects and some considerations concerning the mechanism of RI photodissociation and its relationship to the observed spectral functions are presented. The procedure for the measurement of the quantity $\Phi_{I*}(\lambda)$ is substantiated in more detail than in [3, 5, 11]. The remaining details of the experiment are presented in [3, 5, 11, 14].

3. The Procedure for Measuring $\Phi_{I*}(\lambda)$.

The basic concepts underlying the method for the determination of $\Phi_{I*}(\lambda)$ were set forth earlier in [3-5, 11-14]. The basis of the method is the experimental fact that the reaction rate constants of the atoms $I(^2P_{1/2}) = I^*$ and $I(^2P_{3/2}) = I$ with nitrous chloride differ so greatly (apparently by no less than a factor of 10^4) that during the photolysis of the mixture RI-NOCl-M (M, the third component, is usually a CO_2 molecule), conditions can be created where the I atoms formed during the photodissociation process do not react with the NOCl, but are consumed in other reactions [3, 5, 11]. If in this case, the R radicals which are formed during the photodissociation process likewise do not react with the NOCl, but are consumed via other channels, then the absolute quantum yield, Φ_{NO}, of the NO formation during the photolysis of the RI-NOCl-M mixture is equal to Φ_{I*}. A group theory approach to the analysis of the I* and I reactions with NOCl, because of the lack of information on the properties of the transition complex in these reactions, does not yield, unfortunately, a unique explanation of the great difference in the rate constants. To all apparent extents, the ground states of the products of the reaction of the iodine atoms with NOCl:$NO(^2\Pi)$ and ICl ($^1\Sigma^+$) do not correlate with respect to a smooth surface (without a potential barrier) with the I + NOCl system ($\tilde{X}\ ^1A'$).

We shall show that the conditions indicated here can actually be realized. For this, we shall consider the kinetics of the processes which occur during the photolysis of the mixture RI-NOCl-M (p_{RI} = 3-90 mm Hg, p_{NOCl} < < 0.1 mm Hg, p_M = 0-400 mm Hg, and the intensity of the radiation absorbed by the iodide is $n_{h\nu} \approx 10^{14}$ quanta/($cm^3 \cdot$ sec)).

The main processes which are possible during the photolysis of the given mixture can be described by the following reaction scheme [11]:

$$RJ + h\nu \begin{cases} \nearrow R^* + J^* & (1) \\ \searrow R + J & (1') \end{cases}$$

$$J^* + NOCl \rightarrow NO + JCl \quad (2)$$

$$J^* + RJ \rightarrow J + RJ \quad (3)$$

$$J + NOCl \rightarrow NO + JCl \quad (4)$$

$$J + R\ (+M) \rightarrow RJ\ (+M) \quad (5)$$

$$2J + M \rightarrow J_2 + M \quad (6)$$

$$R^* + M \rightarrow \ldots \rightarrow R + M \quad (7)$$

$$2R\ (+M) \rightarrow R_2\ (+M) \quad (8)$$

$$R + NOCl \rightarrow NO + RCl \quad (9)$$

$$R + JCl \rightarrow RCl + J \quad (10)$$

$$R + J_2 \rightarrow RJ + J \quad (11)$$

$$R + NO\ (+M) \rightarrow RNO\ (+M) \quad (12)$$

(the "hot" radicals are designated with an asterisk). Here, $k_2 \approx 10^{-10}$ cm^3/sec [5, 16]; $k_3 = 3 \cdot 10^{-17} - 4 \cdot 10^{-15}$ cm^3/sec [16, 17]; $k_5 \approx 10^{-11}$ cm^3/sec [15, 18, 19]; $k_6 \approx 10^{-32}$ cm^6/sec^2 when M = CO_2 and 10^{-31} cm^6/sec^2 when M = RI [20, 21]; $k_8 \approx 2 \cdot 10^{-11}$ cm^3/sec for R = CF_3 and $2 \cdot 10^{-12}$ cm^3/sec for R = CF_3CFCF_3 [15, 18-20, 22,23]; $k_{11} \approx 4 \cdot 10^{-12}$ cm^3/sec [24] and $k_{12} < 10^{-13}$ cm^3/sec (from a comparison of data for k_8 and k_{12} for alkyl and perfluoroalkyl radicals). The values of the remaining rate constants are not known. Based on an analysis of the data existing in the literature on the reaction rate constants of alkyl and perfluoroalkyl radicals with Cl_2 and I_2, and from the similarity of the R + NOCl and R + Cl_2 reactions, it can be concluded that the activation energy of reaction (9) and possibly, (10), is greater than zero; to all apparent extents, k_{10} is also greater than k_{12} [20, 24]. The reactions which are not included in the treatment here can be disregarded. It is also obvious that under conditions where the steady-state concentration of [R] is not too low as compared to [I], reaction (6) can be neglected as compared to (5). As it is not difficult to show based on the analysis given below, under our conditions where $p_{RI} \leq 90$ mm Hg and $p_{CO_2} \leq 300$ mm Hg, [R] and [I] are actually comparable. Consequently, reaction (11) can also be disregarded.

Since the rate constants of the processes considered here are high, then at the rates of radiation absorption by iodides of $w_{h\nu} \approx 10^{14}$ quanta/$/(cm^3 \cdot sec)$ which are usually employed in our experiments, the steady-state conditions for [I*], [I] and [R] are established rather quickly

in the initial irradiation period. We shall analyze them assuming that [RI] and [NOCl] are constant and the sum $\Phi_{I^*} + \Phi_I$ is close to 1:

$$\Phi_J \cdot n_{h\nu} = [J^*]\{k_2[NOCl] + k_3[RJ]\}, \tag{13}$$

$$\{k_3[J^*][RJ] + k_{10}[R][JCl] + \Phi_J n_{h\nu} = [J]\{k_4[NOCl] + k_5[R]\}. \tag{14}$$

$$n_{h\nu} = [R]\{k_5[J] + k_8[R] + k_9[NOCl] + k_{10}[JCl] + k_{12}[NO]\}. \tag{15}$$

It is obvious that since [NO] and [ICl] increase during the photolysis process, [R] and [I] should vary with time. Because of the small size of [I] and [R] ($\approx 10^{12}$ cm^{-3}], their rates of change when $n_{h\nu} \approx 10^{14}$ quanta/(cm^3 · sec) are much less than the reaction rates with the participation of I and R (10^{14} cm^{-3} · sec^{-1}). For this reason, equations (13) - (15) should be treated as the quasisteady-state conditions with slowly changing values [NO], [ICl], [I] and [R]. The rate of formation of NO is equal to:

$$\partial[NO]/\partial t = k_2[J^*][NOCl] + k_4[J(t)][NOCl] + [R(t)]\{k_9[NOCl] - k_{12}[NO(t)]\}. \tag{16}$$

Assuming that [I(t)] and [R(t)] = const., the solution of (16) has the form:

$$[NO] = \{\Phi_J \cdot n_{h\nu} k_2[NOCl]\{k_2[NOCl] + k_3[RJ]\}^{-1} + k_4[J][NOCl] + k_9[R][NOCl]\}\{k_{12}[R]\}^{-1}\{1 - \exp\{-k_{12}[R]\}\},$$

which in the case of short photolysis times t yields:

$$[NO]_{t\to 0} = t\{\Phi_J \cdot n_{h\nu} k_2[NOCl]\{k_2[NOCl] + k_3[RJ]\}^{-1} + [NOCl]\{k_4[J] + k_9[R]\}\}, \tag{17}$$

and in the case of long ones:

$$[NO]_{t\to\infty} = \{\Phi_J \cdot n_{h\nu} k_2[NOCl]\{k_2[NOCl] + k_3[RJ]\}^{-1} + NOCl\{k_4[J] + k_9[R]\}\}\{k_{12}[R]\}^{-1} = \text{const.} \tag{18}$$

A similar function can also be derived for ICl.

In the general case, when [R(t)] and [I(t)] ≠ const., the system of equations (13) - (15) cannot be solved analytically, since we do not

have available values of the rate constants for many reactions. However, there is no need for this, since to substantiate the method considered here for the measurement of $\Phi_{I*}(\lambda)$ it is sufficient to demonstrate that with the photolysis of the RI-NOCl-M mixture, for a sufficiently long photolysis time it is always possible to create conditions where [R] and [J] = const. Under these conditions, the function NO = f(t) will have a straight line section which is described by (17). We shall likewise show that one can simultaneously create conditions where the concentrations of R and I are proportional to $n_{h\nu}^a$, where $a < 1$. Then, by increasing $n_{h\nu}$ to such an extent that:

$$[NOCl]\,|k_4[J]+k_9[R]| \ll \Phi_{J*} n_{h\nu} k_2 [NOCl]\,|k_2[NOCl]+k_3[RJ]|^{-1} \qquad (19)$$

(and this is possible, since in this case [J] and [R] $\sim n_{h\nu}^a$, where $a < 1$), and by having studied the slope of the given straight line section under these conditions as a function of the ratio p_{NOCl}/p_{RI}, one can directly measure the quantity $\Phi_{I*}(\lambda)$:

$$\Phi_{J*}(\lambda) = \frac{\partial [NO]}{\partial t n_{h\nu}(\lambda)} \left| 1 + \frac{k_3[RJ]}{k_2[NOCl]} \right|. \qquad (20)$$

We shall demonstrate using a specific example that the straight line section of the function [NO] = f(t) actually occurs and [R] $\sim n_{h\nu}^a$, where $a < 1$. Let $\Phi_{I*} = 1$, $k_5[R] >> k_4[NOCl]$ and $k_3[RI] << k_2[NOCl]$ (the latter inequality under our conditions: $p_{NOCl} \approx 0.1$ mm Hg, $p_{RI} \leq 90$ mm Hg, is always observed for all perfluoroalkyliodides [5, 16, 24]). We shall assume as a first approximation that [ICl] and [NO] change linearly with time: [NO] = [ICl] = $N_{h\nu}t$. Then we derive the following quadratic equation from (15):

$$[R]^2 + [R]\{k_9[NOCl] + (k_{10}+k_{12})\, n_{h\nu} t\} k_8^{-1} - n_{h\nu} k_8^{-1} = 0. \qquad (21)$$

Its positive solution has the form:

$$[R] = -0{,}5\,|k_9[NOCl] + (k_{10}+k_{12})\, n_{h\nu} t\,|k_8^{-1} + \{0{,}25\{k_9[NOCl] + (k_{10}+k_{12})\, n_{h\nu} t\}^2 k_8^{-2} + n_{h\nu} k_8^{-1}\}^{1/2}.$$

In the limiting cases, we find that [25]:

$$[R] = \sqrt{n_{h\nu}/k_8} \text{ при } 0{,}25\{k_9[NOCl] + (k_{10}+k_{12})\, n_{h\nu} t\}\, k_8^{-1} \leqslant n_{h\nu}, \qquad (22) \quad (22)$$

$$[R] = n_{h\nu}\,/\{k_9[NOCl] + (k_{10}+k_{12})\, n_{h\nu} t\}^{-1} \text{ при } n_{h\nu} \leqslant 0{,}6\,|k_8[NOCl] + (k_{10}+k_{12})\, n_{h\nu} t|\, k_8^{-1}. \qquad (23) \quad (23)$$

By making use of the data given above for k_2--K_{12}, it is not difficult to show that when $n_{h\nu} \approx 10^{14}$ quanta/(sec · cm^3) and $t \leq 3$ sec, conditions can be created under which inequality (22) is justified. In fact, since the activation energy for reaction (9) is greater than zero, by thermalizing the R radicals, one can reduce the value of the constant k_9 down to 10^{-14} cm^3/sec. In this case, if $k_{10} \leq 10^{-13}$ cm^3/sec, then $[R] = \sqrt{n_{h\nu}/k_8} = \text{const}$. The greatest possible value of k_{10} cannot introduce distortion into the quantity being measured; when $k_{10} \gg k_{12}$, the linear section described by equation (17), always occurs, as will be demonstrated below. If, as in the case of RI = $(CF_3)_3CI$ [15], the quantity k_8 is anomalously small, then with complete thermalization of the radicals and sufficiently large value of k_{10} and k_{12}, it can be found from (23) that $[R] \sim t^{-1}$. In this case, equation (21) generally loses its meaning; a precise solution is needed for equations (16) and for [ICl] analogous to it. It is not difficult to show that when the conditions of the example considered here are met, one can derive from them the following system of nonlinear differential equations:

$$\partial [NO]/\partial t = n_{h\nu} \{1 - k_{12}[NO(t)]\{k_{10}[JCl(t)] + k_{12}[NO(t)]\}^{-1}\};$$
$$\partial [JCl]/\partial t = n_{h\nu} \{1 - k_{10}[JCl(t)]\{k_{10}[JCl(t)] + k_{12}[NO(t)]\}^{-1}\}.$$

The solution of this system has the form:

$$\Phi_{NO} = 1 = \Phi_{J^*} \quad \text{при} \quad k_{10} \gg k_{12},$$
$$\Phi_{NO} = 0 \quad \text{при} \quad k_{10} \ll k_{12},$$
$$\Phi_{NO} = 1/2 \quad \text{при} \quad k_{10} = k_{12}$$

(the latter is true since ICl and NO are formed in one reaction with the same yield). One can also note that when $k_{10} < k_{12}$, $\partial^2[NO]/\partial t^2 > 0$, and when $k_{10} > k_{12}$, $\partial^2[NO]/\partial t^2 < 0$. Thus, the measurement of Φ when studying RI photodissociation with anomalously low values of k_8($<10^{-13}$ cm^3/sec) can lead to an error in the determination of $\Phi_{I^*}(\lambda)$. There are two ways out of the situation which has been created. The RI-NOCl-M-NO mixture can be subjected to photolysis for one to two minutes ($p_{NO} \approx 10^{-2} - 10^{-1}$ mm Hg) and the I_2 and ICl built up in this manner (up to 0.05 - 0.1 mm Hg). Then, by removing the nitric oxide and subjecting the remaining RI-NOCl-M-ICl-I_2 mixture to photolysis, one can determine Φ_{NO} in the usual manner. Since the concentrations of ICl and I_2 in this case will be rather high and almost constant, then when [NO] << [ICl] and [I_2], the NO concentration will practically not change at all. Consequently, equation (17) will prove to be justified. (The deactivation of I* by I_2 molecules can be disregarded in this case, since $k_2[NOCl] \gg k_{11}[I_2]$ [5, 16], while Cl atoms are formed in the I* + ICl reaction [16], where the chlorine atoms rapidly react with the NOCl with the formation of NO [20]). The second way out, which was

used in studying the photodissociation processes of CH_3I, consists in introducing a radical acceptor into the mixture being photolyzed, for example, butylene [5].

The analysis performed here permits the following conclusions:

1. Conditions can always be created where [R] = const. and the NO concentration increases linearly with time during the photolysis process in accordance with equation (17).

2. The length of the linear section of the function [NO] = f(t) can be increased by removing products from the photolysis region, i.e., by means of mixing and circulating the RI-NOCl-M mixture.

3. The concentration of the [R] radicals is either on the order of $n_{h\nu}^{a}$, where $a < 1$ (condition (22) is met), or is small (where rather large amounts of ICl and I_2 are present in the system).

The consideration of another limiting case, $\Phi_I = I$, which we will not go into here because of a lack of space, makes it possible to come to precisely the same conclusions, and additionally, to demonstrate that with an increase in $n_{h\nu}$, conditions are attainable where $[I] \sim n_{h\nu}^{b}$, where $b < 1$. For this reason, the conditions of the experiment under which equality (19) is observed, i.e., the quantity Φ_{I*} is determined by equation (20), can actually be created.

Thus, if the quantum yield of NO formation, which is determined based on the linear section of the curve NO = f(t), falls off when M is introduced and when $n_{h\nu}$ increases from the maximum possible value $\Phi_{NO} = 2$ to some constant value $\Phi_{NO} \leq 1$, then it can be assumed that all of the radicals have been thermalized and condition (19) is met, i.e., the quantity Φ_{NO} is determined by processes (1) - (3).

The experiment to study $\Phi_{I*}(\lambda)$ usually consisted of the following steps. With two to three quantum energies (we shall call them reference points), the functions NO = f(t) for the RI-NOCl-M mixture with various n and M were usually studied at the edges and the center of the absorption band. The quantity $n_{h\nu}$ can be changed by varying the current through the lamp or p_{RI}. In the latter case, an optically thin RI layer was employed so that the intensity of the radiation absorbed by the iodide was:

$$n_{h\nu} = \frac{-dI_{\text{incident}}}{dx} = -\frac{dI_{\text{погл}}}{dx} = I_0(\lambda)\, p_{RJ} \mu_{RJ}(\lambda)\, 273\, (760T)^{-1} \exp\left[\frac{-\mu_{RJ}(\lambda)\, p_{RJ}\, 273}{760T}\, x\right],$$

where $\mu_{RI}(\lambda)$, $(\text{cm} \cdot \text{atm})^{-1}$ is the RI absorption factor; p_{RI}, mm Hg is the pressure; T, °K is the temperature; x, cm is the distance to the front wall of the cell; $I_0(\lambda)$, quanta/($\text{cm}^2 \cdot$ sec) is the intensity of the radiation falling on the cell) in the front and rear layer of the

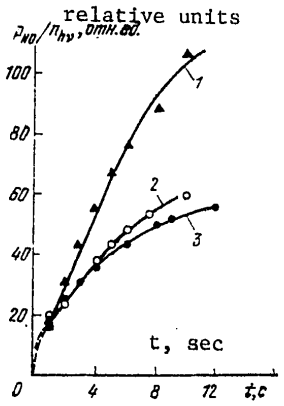

Figure 1. The NO pressure as a function of the photolysis time for the mixture RI-NOCl.

λ = 295 nm; $n_{h\nu} \approx 1.2 \cdot 10^{14}$ quanta/($cm^3 \cdot$ sec);

1. C_3F_7I;
2, 3. CF_3CFICF_3 (curve 3 was obtained with circulation absent).

cell, and was approximately proportional to p_{RI}. For this, the condition $p_{RI}\mu_{RI}(\lambda) < 100$ mm Hg (cm · atm)$^{-1}$ was satisfied (a cell length of 4 cm). The photolysis was usually carried out with a circulation pump turned on which intermixed the mixture in the photolytic cell (approximately half of its volume was illuminated with the light beam) and by gradually removing this mixture from the cell (at a rate of 3 cm^3/sec where V_{cell} = 30 cm^3). Where necessary, experiments on the photolysis of a RI-NOCl-M-ICl-I_2 mixture were also performed.

Typical curves for NO = f(t) are shown in Figure 1. All of the points on the curves were derived using fresh gas mixtures. The NO pressure was measured with a Pirani manometer following the photolysis and the removal of all gases that could be frozen out using liquid oxygen. Where necessary, a mass spectrometer analysis was made of the unfrozen photolysis products.

Three sections can be ascertained in the curves of Figure 1: $t \leq 1$ second - steady-state conditions are established for [I] and [R]; $t \approx 1 - 6$ seconds (curves 1 and 2) and 1 - 4 seconds (curve 3) is a linear section and $t \geq 6$ seconds is the saturation section. The circulation of the mixture, as was anticipated, leads to an increase in the size of the straight line section. When $t \leq 4$ seconds, curves 2 and 3 coincide. All of this confirms the correctness of conclusions 1 and 2.

A typical curve for $\Phi_{NO} = f(n_{h\nu})$ for one of the reference points is shown in Figure 2. It can be seen that an increase in $n_{h\nu}$ actually leads to a reduction in Φ_{NO} down to a certain constant level. The points on the horizontal section of the curve were obtained for various values of p_{RI}, $I_0(\lambda)$ and p_{CO_2}. Beginning at certain critical values of $n_{h\nu}^{cr}$ and p_{total}, the quantity Φ_{NO} ceases to depend on the experimental conditions. All of this proves the correctness of the conclusions drawn earlier. Since in this case, $\Phi_{NO} \neq f(p_{RI}/p_{NOCl})$, something which is in complete agreement with the small value of k3, we are right to assume that in the horizontal section that $\Phi_{NO} = \Phi_{I^*}$. Where there is marked deactivation of I* by the RI molecules (when $p_{CO_2} \leq 300$ mm Hg, the deactivation of I* by CO_2

molecules is only weakly expressed [5]), the functions $\Phi_{NO} = f(p_{RI}/p_{NOCl})$ were studied for the case where $n_{h\nu}/p_{NOCl} > n^{cr}_{h\nu}/0.1$ mm Hg, while the quantity Φ_{I*} was computed from formula (20) [3, 5, 11].

Measurements of $\Phi_{NO} = f(n_{h\nu}, p_M)$ were usually not made at other quantum energies (not reference points), while the quantity $n_{h\nu}$ was chosen within the range of the horizontal section of the curve in FIgure 2. The described procedure was repeated for each new RI. The experimental conditions and the resulting experimental data for one of the iodides studied here are shown in Table 1. The sum $\Phi_{I*} + \Phi_I = 2\Phi_{I_2}$ was determined from results of a study of the photolysis of the mixture RI-NO-M [12, 13].

Results of the Experiment; Discussion

The results of measuring the spectral functions of the absolute quantum yields of the formation of $I(^2P_{1/2})$ atoms are shown in Figure 3. We shall describe the conditions under which they were obtained.

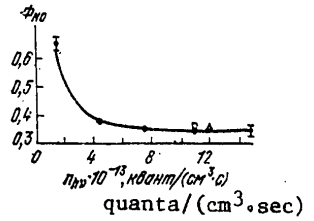

Figure 2. The absolute quantum yield of the formation of NO, obtained for the linear section of the curve NO = f(t) as a function of the quantity $n_{h\nu}$ RI = = CF_3CFICF_3, λ = 275 nm.

The solid black dots are for $I_0 = 0.72 \cdot 10^{15}$ quanta/(cm^2 · sec), $p_{CO_2} = 0$; the triangles are for $I_0 = 1.4 \cdot 10^{15}$ quanta/(cm^2 · sec), p_{CO_2} = 200 mm Hg; the light circles are for $I_0 = 1.25 \cdot 10^{15}$ quanta/(cm^2 · sec), p_{CO_2} = 100 mm Hg.

CF_3I. The CF_3 radicals are more slowly thermalized than the heavier perfluoroalkyl radicals during collisions with RI, and for this reason, it is necessary to introduce CO_2 for their thermalization. As a check has shown, as soon as $p_{CO_2} \geq 100$ mm Hg and $p_{RI} \geq 4$ mm Hg, Φ_{NO} does not depend on p_{CO_2}. All of the data presented in Figure 3 for CF_3I were obtained when p_{CO_2} = 200 mm Hg, p_{RI} = 5 - 50 mm Hg and $n_{h\nu} \geq 0.4 \cdot 10^{14}$ quanta/(cm^2 · sec); at the reference points, $n_{h\nu} = (0.2 - 1.3) \cdot 10^{14}$ quanta/(cm^3 · sec). The mixture of CF_3I-CO_2 captures the NO molecules when it is frozen with liquid oxygen [16]. For this reason, check experiments were run to determine the percentage of NO capture, which, as it turned out, does not depend on p_{NO}. Based on these experiments, the corresponding corrections were introduced into the measured values of Φ_{NO}, where the value of these corrections was small (4.5 - 28% where p_{RI} = 5 to 90 mm Hg respectively, p_{CO_2} = 200 mm Hg).

C_2F_5I. The experimental conditions are shown in Table 1. There is no need to introduce TO_2 for the thremalization of $C_2F_5^*$. A correction of 5% ($p_{C_2F_5I}$ = 4.5 mm Hg) to 24% ($p_{C_2F_5I}$ = 60 mm Hg) for NO capture during freezing was introduced into the value of Φ_{NO}.

C_3F_7I, CF_3CFICF_3, $CF_3OCF_2CF_2I$. The conditions were as follows: p_{RI} = = 4 to 30 mm Hg; $n_{h\nu} \geq 0.7 \cdot 10^{14}$ quanta/($cm^3 \cdot$ sec); at the reference points, $n_{h\nu} = (0.15 - 1.5) \cdot 10^{14}$ quanta/($cm^3 \cdot$ sec), p_{CO_2} = 0 - 300 mm Hg. No NO capture was detected during freezing.

The data shown in Figure for the measured spectral functions $\Phi_I^*(\lambda)$ dose parens + $\Phi_I(\lambda) = 2\Phi_{I_2}(\lambda)$ along with the RI absorption spectra which were measured previously [13] and in this work make it possible to determine the spectral functions of the partial absorption cross-sections corresponding to the transitions to the RI states, which dissociate into R + I*, R + I as well as via channels different from (1) and (1') ($\Phi_{I_2}(\lambda)$ is not equal to 0.5 at all quanta energies, Figure 4). From these data, in turn, one can compute the integral absolute quantum yields:

$$\Phi = \int_{\lambda_1}^{\lambda_2} \mu_{RJ}(\lambda)\,\Phi(\lambda)\,d\lambda \Big/ \int_{\lambda_1}^{\lambda_2} \mu_{RJ}(\lambda)\,d\lambda$$

(λ_1 and λ_2 are the boundaries of the absorption band) of the RI photodissociation products, the oscillator strengths of the corresponding transitions f, the splitting energy ΔE between the excited RI states in the equilibrium configuration of the ground state (Table 2).

TABLE 1

The Experimetal Conditions for the Measurement of the Spectral Dependence of the Absolute Quantum Yield of the Formation of $I(^2P_{1/2})$ During the Photolysis of C_2F_5I

λ, нм nm	$I_0 \cdot 10^{-14}$, квант/(см²·с)	p_{RJ}, мм рт. ст.	p_{CO_2}, мм рт. ст.	$n_{h\nu} \cdot 10^{-14}$, квант/(см³·с)	Φ_J
255	(1) 4,2	mm Hg_{10}	mm Hg_0	(2) 0,7	1,00±0,06
265*	6,6	4,5 — 7,5	0 — 200	0,6 — 1,1	0,98
275	9	6,2	0	0,8	0,93
285	9	15	0	1,3	0,86
295*	9,7	16 — 30	0 — 400	0,7 — 1,3	0,78
305	10	60	0	0,9	0,73

Note: Data obtained where $n_{h\nu} \geq n_{h\nu}^{cr}$ and $P_{obshch} \geq P_{cr}$ are given for the reference points (*).

Key: 1. $I_0 \cdot 10^{-14}$, quanta/($cm^2 \cdot$ sec);
2. $n_{h\nu} \cdot 10^{-14}$, quanta/($cm^3 \cdot$ sec).

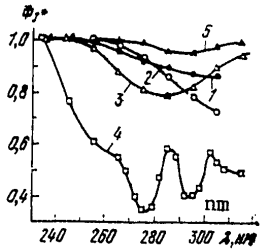

Figure 3. The spectral curves for the absolute quantum yield of the formation of $I(^2P_{1/2})$ during the photodissociation of RI (the measurement error does not exceed 6 percent).

Key: 1. CF_3I;
2. C_2F_5I;
3. C_3F_7I;
4. CF_3CFICF_3;
5. $CF_3OCF_2CF_2I$ (the spectral resolution is about 4 nm).

From our point of view, the interpretation of these data (see Figure 4 and Table 2) can be of great interest. If the mechanism of iodide photodissociation is understood, then one can attempt to predict the value of Φ_{I*} for the photodissociation of iodides which have not yet been studied or not as yet synthesized, and which are promising for any reason for utilization in FIL's. This is a complex question and has been given very little treatment in the literature. Till now, it has not been established which factors - molecule symmetry, radical ionization potential as some authors assume [6, 7] or some other factors - are responsible for the probability of transitions to states which correlate with R + I* and R + I. It is likewise unclear what the mechanism is for the influence of these factors.

The theoretical aspects of the spectroscopic properties of halides were worked out in the 1930's by Mulliken [26-33]; paper [34] can also be cited. There is insufficient space here to allow us to deal with all aspects of this theory which concern the case of large spin-orbital interaction (Gund's case c [35]). We will note only that of the types of bonds ascertained by Mulliken, the case of the Ω-ω bond [28, 30, 36] or the C bond with distant nuclei [27, 28, 30-34, 36] have a direct bearing on the question considered here. The spin quantum number loses its meaning in all of these cases. The mixing of states with identical quantum numbers Λ, Ω (Ω-ω bond) or Ω (C, type I, II), with identical parity (g or u) and identical symmetry properties relative to inversion ("+" or "-") leads to the removal of inhibitions from the transitions which are forbidden in the case of the Λ-S bond. The mixing of the $^3\Pi_1$ and the $^1\Pi_1$ states (in the terms of the Λ-S bond) of a HI molecule is explained by the marked probability of the transition $^3\Pi_1 \leftarrow X^1\Sigma_g^+$ [30, 37]. To explain the relatively large oscillator strength of the transition $^3\Pi_{0_u^+} \leftarrow X^1\Sigma_g^+$ (or $0_u^+ \leftarrow 0_g^+$ in the terms of the C bond) in the I_2 molecule, it is necessary to assume that the ground state of I_2 ($\sigma_g^2\pi_u^4\pi_g^4\sigma_u^0$ - 2440 0_g^+) mixes with the 2341 0_g^+ state lying at 4.1 eV above it, while the 2431 0_u^+ state mixes with the 1441 0_u^+ and 1342 0_u^+ states [33].

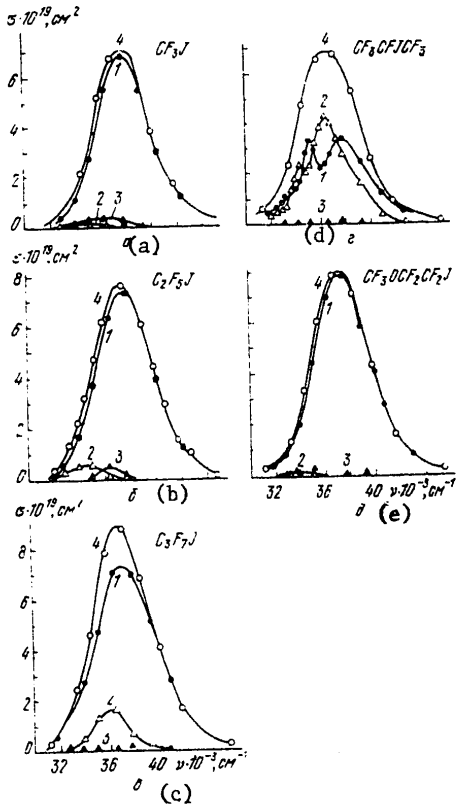

Figure 4. The partial absorption cross-sections, σ_i, corresponding to transitions to states which dissociate into R + I* ($^2P_{1/2}$) (1), R + I ($^2P_{3/2}$) (2) and via other channels (3), as well as the total cross-section, σ_{tot} (4) (the measurement error in σ_i is no more than 8 percent of σ_{tot}; the spectral resolution is $\sigma_i \approx 4$ nm.

A group theory analysis shows that among the lowest excited states of the I_2 molecule, only $^3\Pi_{0u}^+$ correlates with I + I*, while the remaining ones correlate with two I atoms in the ground state (for HI, these are $^3\Pi_0^+$ and $^3\Pi_0^-$, $^1\Pi_1$, $^3\Pi_1$ and $^3\Pi_2$ states respectively). The value of Φ_{I^*} during the photolysis of these molecules is determined both by the type of bond and the interaction of the indicated states between each other and with other states. The existing experimental data are in good agreement with the representations of theory [36, 37].

Mulliken proposed that the nature of the transitions in alkyliodides was the same as in their biatomic analogs [29, 38]. With the absorption of a light quantum by a CH_3I molecule, the transition $...(5p\pi_I e)^3\sigma^* a_1^+, ^3E \leftarrow \leftarrow (...5p\pi_I e)^4\ ^1A_1$ is observed in the first band, in which case the ^3E state, because of the presence of a strong spin-orbital interaction is split into E + E + A_2 + A_1^*, of which only A_1^* correlates with CH_3 + I* [29, 39 (p 295), 40, 41]. The nature and the similarity of the absorption

TABLE 2

RJ	Φ_{J^*}	$\Phi_J + \Phi_{J^*}$	$\Phi_{J^*}/(\Phi_{J^*}+\Phi_J) = P$	P [6, ·]	ρ, при 265 нм	$f_{J^*} \cdot 10^3$	$f_{J^*} \cdot 10^3$	ΔE, см$^{-1}$	q_n	q_{σ^*}	Δq
CF_3J	$0,94^{+0,06}_{-0,07}$	$0,96^{+0,04}_{-0,09}$	$0,98^{+0,02}_{-0,09}$	0,91±0,03	0,91± ±0,005	5,3±1,5	0,1	~4000	0,959	0	0,959
C_2F_5J	$0,94^{+0,06}_{-0,07}$	$0,98^{+0,02}_{-0,09}$	$0,96^{+0,04}_{-0,09}$	0,98	—	5,0±1,5	0,2	~3000	0,964	0,005	0,959
C_3F_7J	0,86±0,07	$0,98^{+0,02}_{-0,07}$	$0,88^{+0,09}_{-0,09}$	0,99	0,978± ±0,12	5,4±1,5	0,9±0,3	~800	0,961	0,236	0,752
CF_3CFJCF_3	0,51±0,05	$0,99^{+0,01}_{-0,09}$	0,52±0,09	0,90± ±0,02	—	2,5±0,8	2,2±0,7	~0	0,580	0,140	0,440
$CF_3OCF_2CF_2J$	$0,98^{+0,02}_{-0,07}$	$0,99^{+0,01}_{-0,07}$	$0,99^{+0,01}_{-0,07}$	—	—	5,3±1,5	0,05	~3500	—	—	—

Note: The confidence level is ≥ 0.90; in calculating the relative error in the determination of the quantities f_{I^*} and f_I, it was assumed that the accuracy in the measurement of the RI absorption factor was about 20%.

spectra of alkyliodides makes it possible to assume that the transition of the $5p\pi_I e$ electron to the antibonding orbital σ^*a_1 leads to the formation of repulsion states, in which case the σ^*a_1 orbital is localized at the C-I bond. All of this made it possible for Mulliken to classify the lower excited states of the alkyliodides as components of a Q-complex, ^1Q, $^3Q_0$, $^3Q_1$ and $^3Q_2$, similar to the $^1\Pi$, $^3\Pi_0$, $^3\Pi_1$ and $^3\Pi_2$ states of the biatomic molecules (for CH_3I, these are the E, $A_1^*(0^+)$, $A_2(0^-)$, E, E states) [39, page 25]. It followed from the data of [42] that the more intense shortwave component of the complex absorption band of CH_3I corresponds to the transition to the state $^3Q_0$. The type of bond in CH_3I is close to the "C type I + type II". We will note that all of the considerations of Mulliken cited above are justified to the same extent for the perfluoro-alkyliodides.

We shall attempt to explain the fact that the probability of a transition to a CF_3I state which dissociates to CF_3 + I* (in following Mulliken, we shall call it $^3Q_0$) is much greater than to a state which dissociates into CF_3 + I (we shall call it $^3Q_1$) (the $^1Q_1$ state, according to Mulliken, is located in the shortwave portion of the first RI absorption band) close parens (see Figure 4a, Table 2). We shall analyze what is responsible for the change in the relationships of the probabilities of transitions to the $^3Q_0$ and $^3Q_1$ states when R changes.

By studying the perturbations of the components of the Q-complex in homonuclear (I_2) and heteronuclear (HI) molecules, one can hypothesize that the intensity of the transitions to the states of the given complex in the CF_3I molecule is determined by the nature of the interaction of these states with higher Rydberg states, the intensity of the transitions to which is almost two orders of magnitude greater. If the observed distribution of the transition intensities in the absorption spectrum of this molecule were due to the disturbance of the $^3Q_0$ state from the other component of the Q-complex having a "singlet" nature in a zero approximation, i.e., $^1Q_1$, then this state should be manifest rather strongly in the CF_3I absorption spectrum. With an increase in the perfluoroalkyl radical, the ratio of the probabilities of transitions to the $^3Q_0$ and $^3Q_1$ states changes, something which entails a change in the quantity Φ_{I*}.

The symmetry selection rules, even in the $C_{\infty v}$ group provide nothing to explain the observed transition probabilities. It is obvious that the explanation of the observed effects should take into account both the nature of the interaction in the Q-complex and the interaction of the states participating in the transition with other states of the IR molecule. Apparently, the latter interaction changes little when R changes, something which is indicated by the practically unchanged oscillator strength of the first absorption bands of the RI molecules. (We will also note that when R changes, the position of the first and subsequent absorption bands changes little [13, 43] and the length of the C-I bond almost does not change at all [44, 45]). Based on what has been said, the conclusion can be drawn that the ratio of the probabilities of the transitions to the $^3Q_0$ and $^3Q_1$ states, and consequently, also the value of Φ_{I*} when R changes are determined by the interaction in the Q-complex.

The decrease in Φ_{I*} in the CF_3I-C_3F_7I series (we shall treat the $CF_3OCF_2CF_2I$ molecule below as a separate special case) is accompanied by a reduction in the energy separation between the $^3Q_0$ and $^3Q_1$ states. It is logical to assume that when these states come close together, they interact with each other (such interaction is permitted even in the $C_{\infty v}$ group by the rules for perturbation selection). In the case of the mixing of the $^3Q_0$ and $^3Q_1$ states, the sum of the oscillator strengths for the transitions to these states remains constant, whereas there is a gradual transfer of oscillator strength from the state with the greatest f to the state with the least f [46].

The amount of splitting between $^3Q_0$ and $^3Q_1$ depends on the length of the C-I bond. It can be anticipated that at certain values of the spacing, the potential surfaces of the indicated states can come closer together, leading to their intersection or repulsion. As we assume, it is specifically this case which is realized in the CF_3CFICF_3 molecule. We noted earlier [14] that the phenomenon of oscillation of the partial absorption cross-sections of this molecule can be explained in principle by the

oscillatory excitation of the CF_3CFCF_3 radical as it is separated from the iodine atom [47, 48]. However, in this case, the more probable mechanism is illustrated in Figure 5. We shall assume that the oscillator strengths for the transition to the noninteracting states $^3Q_0$ and $^3Q_1$ are approximately the same, while the potential surfaces of these states in the region of the vertical transition come close together and repel each other.

Then the spectral curves for the partial absorption cross-sections in the $^3Q_0$ and $^3Q_1$ states will have the form shown in Figure 5. The conclusion concerning the low probability of the diabatic process, i.e., the transition from *a* to *b* and from *c* to *d*, does not contradict existing notions of the mechanism of the interaction of electron states. In fact, in the first case, the interaction of the given states is permitted; in the second case, the surfaces draw closer together at a small angle, since the energy of the vertical transition is markedly greater than the energy of the dissociation of RI into R + I* and R + I, and thirdly, the region of the RI potential energy surface, on which the radiation transition is realized, belongs to approximately the same range of energies as the approach region. All of this, which is in accordance with the Landau-Zener model [49, 50], should lead to a high probability of adiabatic transitions (from *a* to *d* and from *c* to *b*), i.e., to strong repulsion of the surfaces.

It can be assumed that during the photodissociation of CF_3I-C_3F_7I, the drawing together of the repulsion surfaces of RI, which lead to their strong interaction, is absent since their absorption spectra are broken down into two bell curves, where the long wave band corresponds to the lower limit of RI dissociation; it also takes place in HI [30, 37] and apparently, in CH_3I [8].

The change in the amount of splitting ΔE between the states of the Q-complex with a change in the radical can be explained in the following manner. It is well known [51] that spin-orbital interaction in atoms depends greatly on the charge of the nucleus Z and the value of the principal quantum number h:

$$\Delta E_{sl} \sim Z^4/h^3.$$

The constancy of spin-orbital splitting (ΔE ≈ 0.6 eV) in the Rydberg RI series [43] is explained quite well by the fact that it is due for the most part to the unpaired 5p electron of the iodine atom, which remains with the excitation of the other 5p electron in the ns, np or nd orbitals. For the molecules studied here, in the region of the Franck-Condon transition, $\Delta E \leq 0.5$ eV, i.e., it is less than ΔE in the Rydberg series. SInce the first RI absorption band is due to the $n \rightarrow \sigma^*$ transition, the value of the spin-orbital interaction, and consequently,

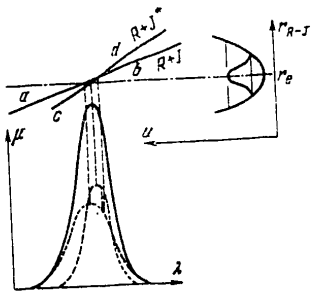

Figure 5. The influence of a quasi-intersection of excited repulsive RI states on the form of the partial cross-sections $\sigma_{I^*}(\lambda)$ and $\sigma_I(\lambda)$.

the splitting of the Q-complex can be determined by how much the excited σ^* orbital is localized around the I atom and has a 5p nature, i.e., by how much the excited electron neutralizes the spin density of the unpaired 5p electron.

For the purpose of ascertaining this hypothesis, we undertook the calculation of the CF_3I, C_2F_5I, C_3F_7I and CF_3CFICF_3 molecules using the MO LCAO SSP method in the semi-empirical CNDO/BW variant [52]. The data on the geometry of the molecules were taken from [44, 45]. A few changes were made in the parameterization system as compared to [52]. The biatomic resonance integrals β_{AB} were computed from the formula $\beta_{AB} = 0.5\ (\beta_{AA} + \beta_{BB})$, where β_{AA} and β_{BB} are the resonance integrals given in [52] for a homonuclear bond. Since we do not have the possibility of going into a complete analysis of the molecular orbitals (MO) within the framework of this paper, we shall cite only the conclusions.

In each of the computed compounds, with the exception of CF_3CFICF_3, one can single out the MO of an unshared pair of an I atom (in the following, the n-MO), consisting basically of $5p_x$-and $5p_y$ atomic orbitals. Given in Table 2 is the total contribution of the $5p_x$ and the $5p_y$ atomic orbitals of iodine to the n-MO (q_n). After the transport of one of the electrons from the n-MO to the first free orbital of the compound, something which corresponds to the $n \rightarrow \sigma^*$ transition, the population of the $5p_x$-and $5p_y$ atomic orbitals of the I atom changes by the amounts q_{σ^*}, which are given in Table 2. Thus, a "portion of an electron" Δq with unpaired spin (see Table 2) remains in the $5p_x$ and $5p_y$ orbitals of iodine. As can be seen from Table 2, the trend towards a change in the size of Δq coincides with the trend of the change in the spin-orbital splitting ΔE.

Thus, within the framework of this calculation, the increase in the 5p nature of the σ^* orbital, i.e., in the time for finding a σ^* electron near an I atom actually leads to a reduction in the quantity $\Delta E = {}^3Q_0 - {}^3Q_1$. It stands to reason that these considerations are of a qualitative nature. We will note that such an interpretation of the observed effects is in agreement with the proposal of the authors of [6, 7] that the size of Φ_{I^*} is greater, the greater the ionization potential of the radical R.

The data of Table 2 show that in terms of its photodissociative properties, the $CF_3OCF_2CF_2I$ molecule is closest to the CF_3I molecule. In light of

the considerations put forward here, it is not difficult to link this to the presence of an oxygen atom in the C-O-C-C chain. In fact, the presence of an oxygen atom in the chain, which has a greater affinity for an electron, should reduce the time for finding a σ* electron near an iodine atom.

A comparison of the values of $\Phi_{I*}/(\Phi_{I*} + \Phi_I)$ from Table 2 with those obtained in papers [6 and 7] reveals marked differences, which are especially significant for the CF_3CFICF_3 molecule. The differences can be due to the reasons discussed earlier [13, 14], as well as the fact that the maximum in the radiation spectrum of the lamp used in [6, 7] possibly falls in the region $\lambda < 250$ nm [53]. This fact markedly improves the agreement of our data and that given in [6, 7] (see Figure 3). The calculations likewise show that under the experimental conditions described in [6, 7], it is necessary to take into account reactions (5) and (8). Neglecting them leads to an increase in Φ_{I*}, which is greater, the higher k_5/k_8 is.

We will note in conclusion that it follows from the data cited here that using molecules in FIL's which have larger radicals than does C_3F_7I does not lead to an increase in the quantity Φ_{I*}. One can anticipate only that there will be a slight positive effect because of the change in the ratio k_5/k_8 in this series.

The authors would like to express their deep gratitude to T.K. Rebana and G.A. Skorobogatov for their useful discussions.

BIBLIOGRAPHY

1. J.V.V. Kasper, G.S. Pimentel, APPL. PHYS. LETTS., 5, 231, (1964).

2. S.J. Riley, K.R. Wilson, FAR. DISC. CHEM. SOC., No 53, 132, (1972).

3. A.M. Pravilov, L.G. Karpov, L.G. Smirnova, F.I. Vilesov, KHIMIYA VYSOKIKH ENERGIY [HIGH ENERGY CHEMISTRY], 7, 335, (1973).

4. L.G. Karpov, A.M. Pravilov, F.I. Vilesov, "Tezisy dokl. II Vsesoyus. soveshchaniya po fotokhimii" ["Abstracts of Reports to the Second All-Union Conference on Photochemistry"], Sukhumi, 1 - 4 October, 1974, p 25.

5. L.G. Karpov, A.M. Pravilov, F.I. Vilesov, KHIMIYA VYSOKIKH ENERGIY, 8, 489, (1974).

6. T. Donohue, J.R. Wiesenfeld, CHEM. PHYS. LETTS., 33, 176, (1975).

7. T. Donohue, J.R. Wiesenfeld, J. CHEM. PHYS., 63, 3130, (1975).

8. A. Gedanken, M.D. Rowe, Chem. Phys. Letts., 34, 39, (1975).

9. R.E. Palmer, T.D. Padrick, J. CHEM. PHYS., 64, 2051, (1976).

10. G.A. Skorobogatov, V.G. Seleznev, O.N. Slesar', V.M. Tret'yak, "Tezisy dokladov III Vsesoyuz. soveshchaniya po fotokhimii" ["Abstracts of Reports to the Third All-Union Conference on Photochemistry"], Rostov-na-Donu, 8 - 11 July, 1977, p 234.

11. L.G. Karpov, A.M. Pravilov, F.I. Vilesov, KVANTOVAYA ELEKTRONIKA, 4, 822, (1977).

12. L.G. Karpov, A.M. Pravilov, F.I. Vilesov, KVANTOVAYA ELEKTRONIKA, 4, 889, (1977).

13. A.M. Pravilov, F.I. Vilesov, V.A. Yelokhin, V.S. Ivanov, A.S. Koslov, KVANTOVAYA ELEKTRONIKA, 5, 618, (1978).

14. A.M. Pravilov, A.S. Koslov, F.I. Vilesov, KVANTOVAYA ELEKTRONIKA, 5, 1161, (1978).

15. L.S. Yershov, V.Yu. Zalesskiy, V.I. Sokolov, KVANTOVAYA ELEKTRONIKA, 5, 865, (1978).

16. R.J. Donovan, D. Husain, CHEM. REV., 70, 489, (1970).

17. S.L. Dobychin, L.D. Mikheyev, A.B. Pavlov, V.P. Fokanov, M.A. Khodorkovskiy, KVANTOVAYA ELEKTRONIKA, 5, 2461, (1978).

18. S.V. Kuznetsova, A.I. Maslov, "Preprint FIAN" ["Preprint of the Physics Institute of the USSR Academy of Sciences], Moscow, 1978.

19. G.A. Skorobogatov, O.N. Slesar', "Abstracts of Reports to the Third All-Union Conference on Photochemistry"], Rostov-na-Donu, 8 - 11 July, 1977, p 233; VESTNIK LGU [BULLETIN OF LENINGRAD STATE UNIVERSITY], No 4, 39, (1979).

20. V.N. Kondrat'yev, "Konstanty skorostey gazofaznykh reaktsiy: Spravochnik" ["Gaseous Phase Reaction Rate Constants: A Handbook"], Moscow, Nauka Publishers, 1970.

21. L.S. Yershov, V.Yu. Zalesskiy, L.N. Kokushkin, KHIMIYA VYSOKIKH ENERGIY [HIGH ENERGY CHEMISTRY], 8, 225, (1974).

22. T. Ogawa, G.A. Carlson, G.C. Pimentel, J. PHYS. CHEM., 74, 2050, (1970).

23. R. Hiatt. S.W. Benson, INT. J. CHEM. KIN., 4, 479, (1972).

24. J.C. Amphlett, E. Whittle, TRANS. FAR. SOC., 62, 1662, (1966).

25. I.N. Bronshteyn, K.A. Semendyayev, "Spravochnik po matematike" ["Mathematics Handbook"], Moscow, Fizmatgiz Publishers, 1957, p 119.

26. R.S. Mulliken, REV. MOD. PHYS., 2, 60, (1930).

27. R.S. Mulliken, REV. MOD. PHYS., 3, 89, (1931).

28. R.S. Mulliken, PHYS. REV., 46, 549, (1934).

29. R.S. Mulliken, PHYS. REV., 47, 413, (1935).

30. R.S. Mulliken, PHYS. REV., 51, 310, (1937).

31. R.S. Mulliken, J. CHEM. PHYS., 8, 382, (1940).

32. R.S. Mulliken, PHYS. REV., 57, 500, (1940).

33. R.S. Mulliken, J. CHEM. PHYS., 55, 288, (1971).

34. J.H. Van Vleck, PHYS. REV., 40, 568, (1932).

35. G. Herzberg, "Spektry i stroyeniye dvukhatomnykh molekul" ["The Spectra and Structure of Biatomic Molecules"], Moscow, Inostrannaya Literatura Publishers, 1949.

36. J.A. Coxon, MOL. SPECTR. CHEM. SOC. (L), 1, 177, (1973).

37. R.D. Clear, S.J. Riley, K.R. Wilson, J. CHEM. PHYS., 63, 1340, (1975).

38. R.S. Mulliken, J. CHEM. PHYS., 3, 506, (1935).

39. G. Herzberg, "Elektronnyye spektry i stroyeniye mnogoatomnykh molekul" ["The Electronic Spectra and Structure of Multiatomic Molecules"], Moscow, Mir Publishers, 1969.

40. L.B. Nikol'skiy, OPTIKA I SPEKTROSKOPIYA, 29, 1049, (1970).

41. M. Dzvonik, J. Yang, R. Bersohn, J. CHEM. PHYS., 61, 4408, (1974).

42. D. Porret, C.F. Goodeve, PROC. ROY. SOC., A165, 31, (1938).

43. R.A. Boshi, D.R. Salahub, MOLEC. PHYS. 24, 735, (1972).

44. A.L. Andreassen, S.H. Bauer, J. CHEM. PHYS., 56, 3802, (1972).

45. L.V. Vilkov, V.S. Mastryukov, N.I. Sadova, "Opredeleniye geometricheskogo stroyeniya svobodnykh molekul" ["The Determination of the Geometrical Structure of Free Molecules"], Leningrad, Khimiya Publishers, 1978, p 125.

46. C.A. Nicolaides, D.R. Beck, CHEM. PHYS. LETTS., 53, 87, (1978).

47. J.A. Beswick, J. Jortner, CHEM. PHYS., 24, I, (1977).

48. R.T. Pack, J. CHEM. PHYS., 65, 4765, (1976).

49. Ye.Ye. Nikitin, USPEKHI KHIMII [PROGRESS IN CHEMISTRY], 43, 1905, (1976).

50. M.S. Child, MOLEC. PHYS., 32, 1495, (1976).

51. E.V. Shpol'skiy, "Atomnaya fizika" ["Nuclear Physics"], Moscow, Nauka Publishers, 1974, Vol 2, p 299.

52. R.J. Boyd, M.A. Whitehead, J. CHEM. SOC. DALTON TRANS., 1, 73, (1972).

53. Yu.G. Basov, S.L. Boldyrev, L.I. Larionov, A.S. Doynikov, G.Ye. Tsvilyuk, KVANTOVAYA ELEKTRONIKA, 2, 1840, (1975).

[165-8225]

8225
CSO: 1862

UDC 621.373.826.038.823

THE CHARACTERISTICS OF A CW ELECTRICAL IONIZATION CO_2 LASER WITH A COOLED WORKING MIXTURE

Moscow KVANTOVAYA ELEKTRONIKA in Russian Vol 7, No 5, May 80 pp 1067-1073
manuscript received 21 Nov 79

[Paper by N.G. Basov, Ye.P. Glotov, V.A. Danilychev and A.M. Soroka, the USSR Academy of Sciences Physics Institute imeni P.N. Lebedev, Moscow]

[Text] It is shown that preliminary cooling of the working mixture in a CW electrical ionization CO_2 laser permits a significant boost in the optimum working pressure (by a factor of 5 to 10) and the specific volumetric energy output (by a a factor of 3 to 5). A configuration is proposed for a laser set-up, in which the refrigeration unit is placed inside the gas dynamic circuit. This configuration permits a significant reduction in the overall dimensions of laser installation.

1. The electrical ionization method makes it possible to provide for stable and homogeneous pumping of active volumes at high pressures in a wide range of pumping pulse widths, right up to the CW mode [1]. However, CW electrical ionization lasers (NEIL) at the present time operate at pressures not exceeding 0.1 atm [2]. This is related to the high threshold pumping power at atmospheric pressure and room temperature. Under these conditions, light fluxes which considerably exceed the maximum beam loading of modern reflectors $J_* \approx 1 - 2$ KW/cm^2, operating in the CW mode, are needed to provide for a sufficiently high effeciency of the laser, η [2].

The specific energy input power in the case of a fixed electron beam current in the adhesion mode is proportional to the pressure p, and in the recombination mode, it is proportional to $p^{3/2}$, and for this reason, increasing the gas pressure leads to a significant increase in the beam utilization efficiency. This is especially important, since the electron beam current density is limited because of the overheating of the separating foil at the 10 μA/cm^2 level (in the plane of the cathode) [2].

It was experimentally shown in paper [3] that preliminary cooling of the laser mixture to a temperature of T = 200 °K improves the performance of pulsed CO_2 lasers by a factor of 1.3 to 1.5. This is related to the sharp reduction in the relaxation rate of the upper 00^01 lasing level when the temperature is reduced. It is shown in this paper that the preliminary cooling of the gaseous mixture in an NEIL permits an increase of 3 to 4 times in the lasing power, something which is determined primarily not by the increase in the efficiency, but rather by the considerable boost in the working pressure of the laser mixture. The fact is that modern devices, which are used for circulation (fan, compressor) provide for a volumetric gas rate of flow independent of the pressure, and for this reason, the mass rate of flow, and consequently, also the output lasing power will be proportional to the working pressure.

2. We shall consider the flow of the laser mixture at an initial velocity u_0 through a rectangular channel with an active length along the optical axis L. The specific pumping power Q is chosen from the condition that the intensity of the laser radiation nowhere exceeds the limiting beam load on the reflectors, J_*. The formulation of the problem corresponds to the maximum permissible output power of an NEIL with a constant electron beam current density along the flow. The system of gas dynamic equations which describe the flow of the laser mixture through the active region in this case has the form:

$$\rho u = \rho_0 u_0, \quad p = \frac{R}{\mu}\rho T,$$

$$p + \rho u^2 = p_0 + \rho_0 u_0^2, \quad Q(x) = Q_0 \frac{\rho_0}{\rho(x)},$$

$$\frac{\gamma}{\gamma - 1}\rho u \frac{d}{dx}\left(\frac{RT}{\mu}\right) - u\frac{dp}{dx} = (1 - \eta_\Phi) Q(x), \qquad (1)$$

where all of the variables with the zero subscript are referenced to the input into the discharge volume; ρ, μ and T are the density, molecular weight and temperature of the gas; γ is the adiabatic exponent; R is the universal gas constant; η_Φ is the physical efficiency of the laser. The energy input power Q is written in the form shown here, since in the adhesion mode which is characteristic of NEIL operation, the electron density does not depend on the gas density (the ionization rate q and the electron extinction rate are proportional to ρ), while the drift velocity is proportional to ρ^{-1}.

At subsonic velocities, the characteristic dimension, for which the laser characteristics are established, is small as compared to the characteristic dimensions for the change in the gas dynamic quantities along the flow. For this reason, in the system of equations which describe the lasing one can neglect the spatial derivatives and write it in the form [4]:

$$\eta_1\eta_2\frac{Q}{h\nu}-(n_2-n_1-n_{1p})\,\sigma_{st}J-\frac{n_2}{\tau_2}=0,$$
$$K\frac{Q}{\varepsilon_1}+2{,}4\,\frac{n_2}{\tau_2}+(n_2-n_1-n_{1p})\,\sigma_{st}J-\frac{n_1}{\tau_1}=0, \qquad (2)$$
$$(n_2-n_1-n_{1p})\,2L\sigma_{st}=\ln\frac{1}{r_1r_2}.$$

Here n_2 and n_1 are the nonequilibrium populations of the upper (00^01) and the lower (1'00) lasing levels; η_1 is the quantum efficiency; η_2 is the fraction of the energy going for the excitation of the vibrational levels of the N_2 and the 00^01 level of the CO_2; $h\nu$ is the laser quantum energy; σ_{st} is the cross-section of the stimulated transitions [4]; $\tau_2 = \tau_2(T)$ is the relaxation time of the 00^01 level (a sharp function of the gas temperature [5]); K and τ_1 are the fractions of the energy going for the excitation and the effective relaxation time of the lower lasing level, taking into account the 01'0, 02^00 and 02^20 levels; r_1 and r_2 are the reflection coefficients of the mirrors; ε_1 is the effective excitation energy of the lower lasing level, averaged with respect to the 01'0, 02^20 and 02^20 [sic] levels.

Because of the fact that the fraction of the energy going into the radiation usually does not exceed 10 to 20%, the quantity $1 - \eta_\Phi$ can be considered constant and equal to 0.85. Then the system of gas dynamic equations (1) ceases to depend on the parameters of the laser radiation and its solution is written in the form:

$$x=\frac{\rho_0u_0^3}{0{,}85Q_0}\left[\frac{\gamma}{\gamma-1}\left(1+\frac{1}{\gamma M_0^2}\right)\ln\frac{u}{u_0}-\frac{\gamma+1}{\gamma-1}\left(\frac{u}{u_0}-1\right)\right],$$
$$\frac{T}{T_0}=\frac{u}{u_0}\left[1-\gamma M_0^2\left(\frac{u}{u_0}-1\right)\right], \qquad (3)$$

where M_0 is the Mach number at the input to the discharge chamber. Knowing the distribution of the gas dynamic quantities, the distribution of the laser parameters along the flow can be calculated:

$$J(x)=\frac{2L\eta_1\eta_2}{\ln(1/r_1r_2)}\left\{Q(x)\left[1-\frac{\tau_1/\tau_2}{1-1{,}4\tau_1/\tau_2}\left(1+\frac{K}{\eta_1\eta_2}\frac{h\nu}{\varepsilon_1}\right)\right]-Q_*\right\}, \qquad (4)$$

where the value of the maximum light flux, $J_m = J_{max}(x)$ is related to the beam strength J_* by the relationship $J_m = J_*(1+r_1)$. The value of the threshold energy input power Q_* is given by the expression:

$$Q_*(x) = \frac{1}{\eta_1\eta_2}\frac{h\nu}{\tau_2}\frac{1}{1-1{,}4\tau_1/\tau_2}\left[\frac{\ln(1/r_1r_2)}{2L\sigma_{st}} + n_{1p}\right]. \qquad (5)$$

At pressures p greater than about 0.1 to 2 atm (depending on the composition of the mixture and the intial temperature), the maximum light flux J_m is already achieved at the input to the active volume. This is related to the fact that at an energy input power on the order of the threshold value, the rise in Q due to the rarefaction of the gas along the flow is smaller than the increase in Q_* due to heating. In this case, Q_0 is determined from the condition $J_0 = J_m$. At low pressures of $p \leq 0.1$ atm, the threshold pumping power at the input is $Q_*(0) \ll Q_0$. For this reason, the initial rise in the energy input, which is related to the reduction in the gas density, becomes a decisive factor and leads to the initial rise in the level of the light flux down stream with respect to the flow. However, in having reached the maximum, J(x) thereafter falls off sharply because of the later strong rise in $Q_*(x)$. The quantity Q_0 is determined from the transcendental equation:

$$J_m = \frac{2L\eta_1\eta_2}{\ln(1/r_1r_2)}\left\{Q(x_m)\left[1 - \frac{\tau_1(x_m)/\tau_2(x_m)}{1-1{,}4\tau_1(x_m)/\tau_2(x_m)}\right] - Q_*(x_m)\right\}, \qquad (6)$$

where the point at which the maximum light flux J_m is achieved is found from the condition $dJ/dx = 0$.

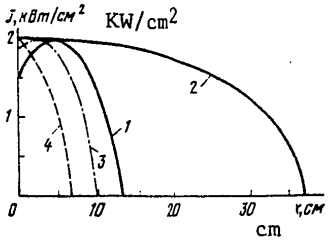

Figure 1. The distribution of the laser radiation intensity along the flow; the gas velocity at the input is u_0 = 100 m/sec.

The distributions of the radiation intensity along the flow are shown in Figure 1 for a laser mixture of CO_2:N_2:He = 1:5:4 at values of $\ln(r_1r_2)^{-1} = 1$ and L = 2m. Since the maximum light flux is limited by the quantity J_m, the maximum volumetric specific energy output is determined by that size at which the lasing is broken off. Curve 1 corresponds to the optimum pressure of $p \approx 0.05$ atm at an initial temperature of T_0 = 300 °K (curves corresponding to T_0 = 300 °K and pressures of p = 0.1 atm (curve 3) and 0.2 atm (curve 4) are shown for the sake of comparison). In this case, the lasing breaks off at a distance of $l \approx 13$ cm. When T_0 is lowered down to 200 °K (curve 2), the optimum pressure is increased up to $p_0 \approx 0.4$ atm, and the dimension of the lasing region is increased up to $l \approx 37$ cm, while the maximum specific energy output, which is determined by the area underneath the distribution curve, more than triples. With a further reduction in the initial temperature, the values of the optimum pressure and the volumetric specific

energy output rise even more. However, at a temperature T_0 < 170 - 200 °K, the CO_2 begins to condense and precipitate out. We will note that the operational mode of an NEIL with a low energy output from the viewpoint of efficiency is not an optimal mode, since at the end of the lasing region, the fraction of the energy input which goes into radiation falls off sharply. For this reason, to obtain a high efficiency, the length of the active region along the flow should not exceed $l \approx 25$ cm (for curve 2). The specific energy output in this case drops off by no more than 20 to 25%.

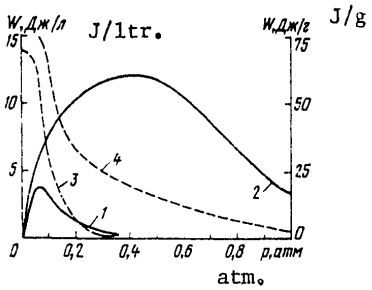

Figure 2. The maximum energy outputs as a function of the gas pressure at the input to the discharge chamber; L, u_0, $\ln(1/r_1r_2)$ and the composition of the mixture are the same as in Figure 1.

Shown in Figure 2 as a function of pressure are the maximum specific volumetric (solid curves) and mass (dashed curves) energy outputs at room temperature (T_0 = 300 °K, curves 1 and 3) and cryogenic temperatures (T_0 = 200 °K, curves 2 and 4). The energy output per unit mass falls off monotonically, since the power of the relaxation losses increases as the square of the pressure. The drop in the rate of the relaxation losses when the temperature is reduced leads to the fact that curve 4 falls above curve 3. The curves for the energy output per unit volume have maxima, since the volumetric energy output is proportional to the product of the pressure times the enrgy output per unit mass of the gas being pumped through. A comparison of curves 1 and 2 shows that when making the transition to the cryogenic temperature, the optimal pressure increases by a factor of 8 ($p_0 \approx$ ≈ 0.4 atm). However, the value of the maximum specific energy input increases only by a factor of 3.5 in this case, something which is due to the increase in the relaxation losses with the rise in the pressure. The maximum volumetric energy output at T = 200 °K amounts to $W_M \approx 12.5$ KJ/m^3. We will note that with the cryogenic gas temperature at the input to the active region, CW laser operation is possible even at atmospheric pressure.

The optimum working pressure (curve 1) and the maximum specific energy output (curve 2) are shown in Figure 3 as a function of the temperature T_0 at the input to the active volume. It can be seen that the value of the optimum pressure increases in step with the reduction in T more sharply than the specific energy output. This is related to the fact that with the rise in pressure, the temperature at which the lasing is broken off drops. It is important to note that in the case of operation using the traditional configuration (T_0 close to room temperature), it is necessary to see that the gas temperature at the output from the heat

exchanger is as close as possible to the temperature of the coolant, although this also leads to a significant increase in the overall dimensions of the laser installation. Thus, for example, increasing T_0 from 242 up to 290 °K leads to a reduction in the volumetric energy output by a factor of 2.

3. Liquid nitrogen can be used to cool the gas down to -70°C, as is done in a CO electroionization laser [1]. However, the use of nitrogen cooling involves considerable engineering difficulties, which are related to the significant increase in the overall dimensions of the installations and the substantial increase in their structural complexity. Because of the large mass rate of flow of liquid nitrogen during continuous operation of the laser, it becomes necessary to design a special cryogenic complex, including a station for the production of liquid nitrogen.

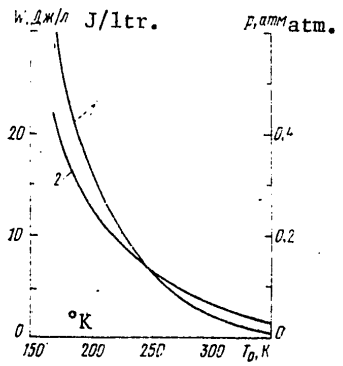

Figure 3. The optimum working pressure (1) and the maximum specific energy output (2) as a function of the temperature at the input to the active volume.

A scheme is proposed in this paper for a laser installation in which the refrigerator is realized inside the gas dynamic loop. In this case, the gas is cooled at the input to the active volume down to a temperature considerably lower than that of the coolant. This makes it possible to substantially reduce the overall dimensions of the unit.

A schematic of a laser unit operating in a refrigeration cycle is shown in Figure 4. The lasing mixture, which is heated in dishcarge chamber 1, is fed to compressor 2 with a compression ratio of P_k, where it is adiabatically compressed and fed to heat exchanger 3 (in the case where a multistage compressor is used, the heat exchangers can be positioned after each compressor stage; in this case, the compression process is close to isothermal). After the heat exchanger, the gas continues to be cooled in turbine 4 as a result of the work done by it A_T. This work can be used to partially compensate for the energy needed to compress the gas in the compressor. The energy removed in the heat exchanger per unit mass exceeds the energy introduced in the discharge by the amount of the difference in the work of the compressor A_k and the work of the turbine, since the preliminary cooling of the gas down to a temperature less than that of the coolant requires the expenditure of work. This leads to a certain reduction in the technical efficiency, the level of which in this case is determined from the formula

$$\eta_T = \frac{Q_c}{Q_p + \dot{m}(A_K - A_T) + Q_\Pi} = \frac{\eta_\Phi}{1 + \dot{m}(A_K - A_T)/Q_p + Q_\Pi/Q_p}, \qquad (7)$$

where Q_p, Q_c and Q_Π are the laser radiation power, the power introduced into the discharge and that delivered to the electron gun respectively; $\eta_\Phi = Q_c/Q_p$ is the physical efficiency; $\dot{m}$ is the mass rate of flow.

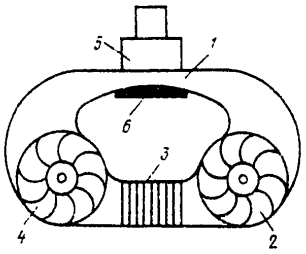

Figure 4. Schematic of an NEIL [CW electrical ionization laser] with turbocompressor cooling of the laser mixture.

Key: 1. Discharge chamber;
2. Axial flow compressor;
3. Heat exchanger;
4. Turbine;
5. Electron gun;
6. Anode of the discharge chamber.

Characteristic thermodynamic cycles are shown in Figure 5 using the example of the "laser refrigerator" with heating in the discharge chamber up to a temperature not exceeding the room temperature. These modes correspond to a high lasing efficiency η_Φ, which is close to the maximum. The cycles in Figure 5a are plotted in p-V coordinates and in Figure 5b-c, in p*-T* coordinates. Here, V is the specific volume; $p^* = p(1 + (\gamma-1)M^2/2)^{\gamma/\gamma-1}$, $T^* = T(1 + (\gamma-1)M^2/2)$ are the stagnation pressure and temperature respectively. The solid curves correspond to an adiabatic compressor and heat exchanger in the high pressure chamber. This configuration makes it possible to reduce the volume of the refrigerator to a minimum, where this determines the overall dimensions of the unit, since the cooling takes place very efficiently. This is related to the large temperature difference between the coolant (room temperature) and the lasing mixture, as well as to the high gas density. The dashed curves correspond to an isothermal compressor, which makes it possible to realize a refrigeration cycle with minimum losses in the technical efficiency.

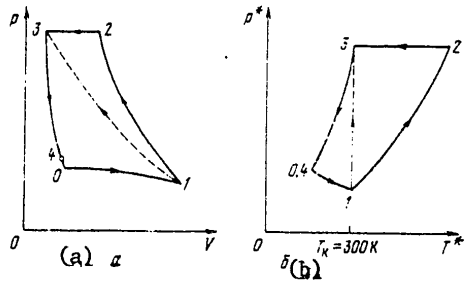

Figure 5. The thermodynamic cycles of the laser installation with turbocompressor cooling in p-V (a) and p*-T* (b) coordinates.

Section 0--1 corresponds to heating of the lasing mixture in the active region, where the stagnation pressure falls off during the heating process:

$$\frac{p_1^*}{p_0^*} = 1 - \frac{(\gamma/2)M_0^2}{1+(\gamma/2)M_0^2}\left(\frac{u_1}{u_0} - 1\right). \tag{8}$$

The final velocity of the gas at the output from the discharge chamber, u_1, is related to the specific energy input by the expression:

$$\frac{W}{c_p T_0} = \gamma M_0^2 \left\{\left(1 + \frac{1}{\gamma M_0^2}\right)\left(\frac{u_1}{u_0} - 1\right) - \frac{\gamma+1}{2\gamma}\left[\left(\frac{u_1}{u_0}\right)^2 - 1\right]\right\}. \tag{9}$$

For the operating mode computed here, the total pressure loss in the discharge chamber does not exceed 10 to 15 %. Section 1--2 corresponds to gas compression in the compressor, 2--3 to isobaric cooling in the heat exchanger, 3--4 to adiabatic gas work in the turbine and 4--0 corresponds to adiabatic acceleration of the gas up to the initial velocity u_0. The points 4 and 0 coincide on the p*-T* diagram.

We shall designate the ratio of the difference between the compressor and turbine powers $N_K - N_T$, to the power introduced into the discharge as η_x. In the case of an adiabatic compressor

$$\eta_x = \frac{c_p T_0}{W}\left\{\left(1 + \frac{W(1-\eta_\Phi)}{c_p T_0}\right)\left[\left(\frac{p_0^*}{p_1^*}\right)^{(\gamma-1)/\gamma}\frac{T_x}{T_0^*} - 1\right] - \left(\frac{T_x}{T_0^*} - 1\right)\right\}, \tag{10}$$

where T_x is the temperature at the refrigerator output. In the case of low Mach numbers at the input to the discharge chamber, formula (10) is considerably simplified, something which is usually observed for ($T_0^* \approx T_0$):

$$\eta_x = [(T_x - T_0^*)/T_x](1-\eta_\Phi). \tag{11}$$

The quantity η_Φ is inserted in the formula for η_x, since the power $Q_p\eta_\Phi$ is removed from the discharge chamber in the form of the laser radiation. Consequently, the expenditures of work for the realization of the refrigeration cycle are lower, the higher the lasing efficiency. When $T_0^* = 200$ °K, $T_x = 300$ °K, $W = c_p(T_x - T_0) = 125$ J/g, $p_1^*/p_0^* = 0.91$ $\eta_x = 0.38$. This leads to a reduction in the technical efficiency as compared to the physical efficiency by a factor of 1.4 ($Q_\pi/Q_p = 0.02$). The value of η_T in this case is 17.7%.

Increasing the difference between the gas temperature at the output from the refrigerator and the coolant temperature up to 100 °K leads to a reduction in the technical efficiency as compared to the physical efficiency by a factor of 1.75. The volume of the refrigerator is reduced by an order of magnitude in this case, while the overall technical efficiency is kept rather high - 14.3%. Consequently, the configuration considered here is a promising one for the design of advanced installations, since modern industrial aviation compressors and turbines, which provide for the requisite mass rates of flow and compression ratio have small overall dimensions [5].

In stationary technological laser installations, it is advantageous to utilize isothermal compressors. In this case, it is expedient to heat the laser mixture no less than up to room temperature: $W \geq c_p(T_x - T_0)$. Assuming the Mach number at the input to the discharge chamber to be low, we obtain the following expression for η_x:

$$\eta_x = \frac{1-\eta_\Phi}{1-T_0/T_x}\left[\ln\frac{T_x}{T_0} - 1 + \frac{T_0}{T_x}\right]. \qquad (12)$$

When T_x = 300 °K, T_0 = 200 °K, η_Φ = 0.25 and η_x = 0.25. The technical efficiency η_T, reaches about 20% in this case.

In laser systems where the optimal lasing temperatures are substantially lower than room temperatures (for example, those using CO), it is possible to combine adiabatic and isothermal compression: below room temperature, the compression is accomplished adiabatically, and thereafter, isothermically.

4. To sum up. It is shown in this paper that cooling of molecular laser mixtures leads to a significant improvement in the specific lasing power of an NEIL by virtue of the increase in the working pressure. In the case of CO_2 laser, cooling the gas down to T = 200 °K makes it possible to boost the pressure by a factor of 8 and increase the specific volumetric energy output by a factor of 3.5. In this case, there is a substantial increase in the utilization efficiency of the electron beam. A fundamentally new configuration is proposed for a laser, in which the refrigerator is realized inside the gas dynamic loop. This circuit permits a significant reduction in the overall dimensions.

We would like to express our gratitude to V.N. Koterov and S.G. Perlov for their useful discussions.

BIBLIOGRAPHY

1. V.A. Danilychev, O.M. Kerimov, I.B. Kovsh, in the book, "Radiotekhnika" ["Radio Engineering"], Moscow, All-Union Institute of Scientific and Technical Information, 1977, Vol 12.

2. N.G. Basov, I.K. Babayev, V.A. Danilychev, M.D. Mikhaylov, V.K. Orlov, V.V. Savel'yev, V.G. Son, N.V. Cheburkin, KVANTOVAYA ELEKTRONIKA, 6, 772, (1979).

3. D.H. Douglas-Hamilton, R.M. Feinberg, R.S. Lowder, J. APPL. PHYS., 46, 3566, (1975).

4. B.F. Gordiyets, A.I. Osipov, Ye.V. Stupochenko, L.A. Shelepin, UFN [PROGRESS IN THE PHYSICAL SCIENCES], 108, 655, (1972).

5. M.M. Maslennikov, Yu.I. Shal'man, "Aviatsionnyye gazoturbinnyye dvigateli" ["Aviation Gas Turbine Engines"], Moscow, Mashinostroyeniye Publishers, 1975.

[165-8225]

8225
CSO: 1862

UDC 621.373.826.038.825.3

A HIGH EFFICIENCY PULSE PERIODIC LASER USING CONCENTRATED NEODYMIUM PHOSPHATE GLASS

Moscow KVANTOVAYA ELEKTRONIKA in Russian Vol 7, No 5, May 80 pp 1120-1122
manuscript received 14 Dec 79

[Paper by A.G. Avanesov, Yu.G. Basov, V.M. Garmash, B.I. Denker, N.N. Il'ichev, G.V. Maksimova, A.A. Malyutin, V.V. Osiko, P.P. Pashinin, A.M. Prokhorov and V.V. Sychev, USSR Academy of Sciences Physics Institute imeni P.N. Lebedev, Moscow]

[Text] A highly efficient pulse periodic laser using concentrated Li-Nd-La phosphate glass has been built which operates in a free running mode with an efficiency of up to 4%. An average output power of 14.5 watts was obtained at a pulse repetition rate of 8 Hz.

At the present time, lasers with YAG:Nd active elements occupy a dominant position in pulse periodic and CW systems. This is explained by the successful combination of a number of parameters in YAG:Nd : the high value of the lasing transition cross-section, σ, and the comparatively long lifetime, something which assures a low lasing threshold. The high thermal conductivity of garnet crystals leads to a rather efficient specific heat removal, however, the low concentration of neodymium and the narrow absorption bands make it possible to use only a small portion of the radiation spectrum of the pumping lamps ($\approx$ 7%), something which limits the actual efficiency in lasers of this type to a level of 1 to 2%. In standard neodymium glasses, just as in silicate and phosphate glasses, despite the low neodymium concentration, the wide absorption bands make it possible to more efficiently utilize the pumping radiation spectrum. A high efficiency, about 4%, has been successfully attained in them, but only in rather large active elements, where the effective absorption in the wide bands is assured by the thickness of the sample. However, by virtue of the low thermal conductivity coefficient, such systems can operate either in a single pulse mode, or at very low repetition rates.

The development of highly concentrated neodymium phosphate glasses [1, 2], in which intense and wide absorption bands assure efficient pumping

absorption at very small thicknesses, has opened up the possibility for the design of laser systems with high efficiencies where small active elements are used. In this case, despite the low thermal conductivity coefficient of the glass, it proves possible to provide for a rather high specific heat removal because of the small dimensions.

The first experiments [3 - 5] with concentrated Li-Nd-La phosphate glass (KNFS) soon demonstrated its promise for use in pulse periodic lasers. A comparison of the lasing characteristics of KNFS with YAG:Nd under similar conditions (optimized for YAG:Nd) [6] confirm the possibility of substituting active elments of KNFS in a number of lasers for the YAG:Nd crystals which are labor intensive with respect to the fabrication technology; this substitution, along with reducing the cost of the lasers, also allows for an improvement in their radiation output parameters. At the present time, the efficiency of domestically produced lasers operating in a pulse periodic mode and using neodymium glass does not exceed 1% at repetition rates of 5 to 8 Hz and the maximum output power is 5 to 8 watts [7, 8]. Of the foreign laser glasses, Q-88 has the greatest efficiency (about 2%) in the pulsed mode [9]. The destruction of the active element with an increase in the pumping power, as well as thermal-optical effects in the active element which lead to substantial distortions of the resonator impede the achievement of high output powers.

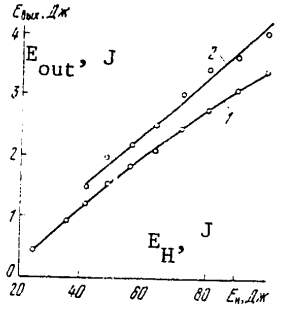

Figure 1. The output energy as a function of the pumping energy.

The utilization conditions for KNFS in pulse periodic lasers are optimized in this paper, something which has made it possible to design a highly efficient laser using this glass, which operates in a free lasing mode.

Active elements of KNFS were used with a neodymium ion concentration of about $8 \cdot 10^{20}$ cm^{-3} and dimensions of 5 x 70 mm and 6.3 x 100 mm in diameter. The luminescence decay time constant in this glass is 180 microseconds. The end faces of the active elements were not transilluminated. The side surface was etched to a depth of 50 to 100 micrometers to imrove the heat resistance. The pumping was accomplished using an ISP-2500 flashlamp. The discharge circuit was formed by a capacitor of C = 200 μFd and an inductance of L = 50 μHy. The current pulse waveform was close to a bell shape with a width at the base of about 300 microseconds. A quartz monoblock with a silver coating served as the reflector. The active element, the flashlamp and the monoblock were cooled with distilled water. The ultraviolet portion of the spectrum was not eliminated from the pumping flashlamp radiation.

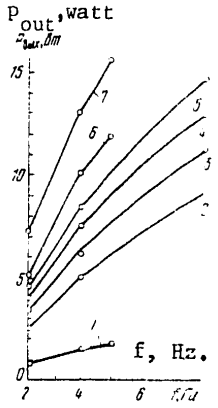

Figure 2. The average output power as a function of frequency at pumping energies of 25 (1), 42 (2), 50 (3), 56 (4), 64 (5), 72 (6) and 100 J/pulse (7).

For an active element with dimensions of 5 x 70 mm in diameter, the laser resonator was formed by a spherical mirror with a radius of curvature of 5 m and a reflection factor of about 100% and a plane mirror with a reflection factor of about 50%. For the active element with dimensions of 6.3 x 100 mm in diameter (a portion of the active elements 60 mm long was illuminated with the pumping radiation), the resonator was formed by a spherical mirror with a radius of curvature of 5 m and a reflection factor of 60% and a plane mirror with a reflection factor of about 100%. The length of the resonator was 250 mm.

Shown in Figure 1 are the lasing energies as a function of the pumping energies for active elements with dimensions of 5 x 70 mm in diameter (1) and 6.3 x 100 mm in diameter (2). The maximum dynamic efficiency for the active element 5 x 70 mm in diamter is 4.5% while the maximum absolute efficiency is 3.2%. With a pumping energy of about 100 J, the curve for the output energy as a function of the pumping energy has a bend which is apparently related to the mismatching of the flashlamp radiation spectrum and the absorption spectrum of the active element. We will also note the fact that at a pumping energy of about 100 J, the active element lased at its own end faces. For an active element with dimensions of 6.3 x 100 mm in diameter, an absolute efficiency of 4.1% was achieved. The efficiency of 4% was achieved at a pumping energy of as low as 60 J.

An active element 5 x 70 mm in diameter was studied in the pulse periodic mode. The family of curves which show the output power as a function of the pumping pulse repetition rate is shown in Figure 2. The energy of the pumping pulse is fixed along each of the curves. Special measures were not taken to correct the thermal lens which arises in the active element during the transition from single pulses to a repetition mode. At the same time, the maximum pulse repetition rate of 8 Hz corresponds to a lasing efficiency which is 15 to 20% less over all than in the single pulse mode, something which attests to the rather good thermo-optical characteristics of KNFS.

In a frequency range of 5 to 8 Hz, a laser output power of 15 $\pm$ 0.5 watts corresponds to an average pumping power of 500 watts. Right up to the pumping power close to the threshold of destruction of the active elements (about 600 watts), the rise in the radiation output power is practically linear.

The type of flashlamp and the pumping pulse width, the geometrical dimensions of the monoblock and the active element as well as the reflection factor of the output reflector were varied in optimizing the laser. We will note that the parameters obtained for the laser markedly exceed the values achieved in a similar system using Q = 88 glass [9] and in a system based on the best domestically produced phosphate glasses with dimensions of the active element of 10 x 130 mm in diameter [10]. The fact that despite the rather high specific pumping power and the lack of filtering of the ultraviolet portion of the pumping spectrum, there was degradation of the laser parameters after about 10^5 bursts is extremely promising. The attainment of a high efficiency in the system considered here and the obtaining of rather high output characteristics of the laser with extremely moderate loads on the flashlamp as compared to its nominal rating demonstrates the possibility of sharply increasing the service life and reliability of such systems.

The studies performed here convincingly demonstrate that KNFS's open up new possibilities for the design of highly efficient pulse periodic laser systems and can find the most widespread applications in the immediate future.

BIBLIOGRAPHY

1. S.Kh. Batygov, Yu.K. Voron'ko, B.I. Denker, A.A. Zlenko, A.Ya. Karacik, G.V. Maksimova, V.B. Neustruyev, V.V. Osiko, V.A. Sychugov, I.A. Shcherbakov, Yu.S. Kuz'minov, KVANTOVAYA ELEKTRONIKA, 3, 2243, (1976).

2. Yu.K. Voron'ko, B.I. Denker, A.A. Zlenko, A.Ya. Karasik, Yu.S. Kuz'minov, G.V. Maksimova., V.V. Osiko, A.M. Prokhorov, V.A. Sychugov, G.P. Shipulo, I.A. Shcherbakov, DAN SSSR [REPORTS OF THE USSR ACADEMY OF SCIENCES], 227, 75, (1976).

3. K.L. Vodop'yanov, B.I. Denker, G.V. Maksimova, A.A. Malyutin, V.V. Osiko, P.P. Pashinin, A.M. Prokhorov, KVANTOVAYA ELEKTRONIKA, 5, 686, (1978).

4. B.I. Denker, A.V. Kil'pio, G.V. Maksimova, A.A. Malyutin, V.V. Osiko, P.P. Pashinin, A.M. Prokhorov, I.A. Shcherbakov, KVANTOVAYA ELEKTRONIKA, 4, 688, (1977).

5. B.I. Denker, V.V. Kil'pio, G.V. Maksimova, A.A. Malyutin, V.V. Osiko, P.P. Pashinin, A.M. Prokhorov, I.A. Shcherbakov, "Tezisy dokl. I Vsesoyuz. konf. 'Optika lazerov'" ["Abstracts of Reports to the First All-Union Conference "Laser Optics'"], Leningrad, GOI [State Institute of Optics imeni S.I. Vavilov] Publishers, 1977, p 15.

6. A.G. Avanesov, I.V. Vasil'yev, Yu.K. Voron'ko, B.I. Denker, S.V. Zinov'yev, A.S. Kuznetsov, V.V. Osiko, P.P. Pashinin, A.M. Prokhorov, A.A. Semenov, KVANTOVAYA ELEKTRONIKA, 6, 1588, (1979).

7. A.A. Mak, V.M. Mit'kin, V.N. Polukhin, A.I. Stepanov, O.S. Shchavelev, KVANTOVAYA ELEKTRONIKA, 2, 850, (1975).

8. N.Ye. Alekseyev, V.V. Gruzdev, A.A. Izyneyev, Yu.L. Kopylov, V.B. Kravchenko, Yu.S. Milyavskiy, Yu.N. Mikhaylov, S.P. Rozman, A.M. Fisher, KVANTOVAYA ELEKTRONIKA, 5, 2354, (1978).

9. John D. Meyers, OPTICAL SPECTRA, No 5, (1977).

10. V.B. Kravchenko, Yu.P. Rudnitskiy, KVANTOVAYA ELEKTRONIKA, 6, 661, (1979).

8225
CSO: 1862

LASER SYSTEMS

Novosibirsk LAZERNYYE SISTEMY in Russian 1980 signed to press 17 Dec 79

[Annotation and table of contents from a collection of articles edited by Veniamin Pavlovich Chebotayev, Nauka, 2500 copies, 208 pages]

[Text] This collection includes articles devoted to experimental and theoretical investigations of resonant frequency conversion in gases and metal vapor, the construction of high-power laser systems based on solid-state and gaseous lasers with electron beam pumping and narrow-band tunable lasers in the visible and near ir regions, and the use of these lasers to solve a number of spectroscopic problems. Some of the articles discuss lasers used in photochemistry.

The book will be of interest to specialists working on the problems of constructing lasers.

TABLE OF CONTENTS

III. Laser Photochemistry

9370
CSO: 1862

MANY-PHOTON IONIZATION OF ATOMS

Moscow MNOGOFOTONNAYA IONIZATSIYA ATOMOV (TRUDY ORDENA LENINA FIZICHESKOGO INSTITUTA imeni P. N. LEBEDEVA AKADEMII NAUK SSSR) [Works of the Lebedev Institute of Physics of the Academy of Sciences USSR] in Russian, Vol 115, 1980

[Annotation and table of contents from a collection of articles edited by Prof. M. S. Rabinovich, Nauka, 1300 copies, 176 pages]

[Text] This collection covers theoretical and experimental research into the phenomenon of atomic ionization in strong light fields. Most of the attention is given to direct and resonant many-photon ionization processes. Modern methods for calculating many-photon cross sections are discussed in detail; optimum methods are revealed by comparing the calculations to experiment. The general theory of ionization in the presence of intermediate resonance is discussed. Different effects determining the width of the resonance state in a strong field are analyzed. The results of an investigation into the perturbation of an atomic spectrum by the method of resonant photon ionization are given. The role of laser radiation statistics in many-photon processes is discussed.

TABLE OF CONTENTS

9370
CSO: 1862

RECOMBINATION LUMINESCENCE AND LASER SPECTROSCOPY

Moscow REKOMBINATSIONNAYA LYUMINESTSENTSIYA I LAZERNAYA SPEKTROSKOPIYA (TRUDY ORDENA LENINA FIZICHESKOGO INSTITUTA IMENI P. N. LEBEDEVA AKADEMII NAUK SSSR) in Russian Vol 117, 1980 signed to press 6 Feb 80 pp 2, 145

[Annotation and Table of Contents from the collection edited by Academician N. G. Basov, Izdatel'stvo Nauka, 1,650 copies, 146 pages]

[Text] The volume is devoted to various aspects of the kinetics of luminescence of crystal-phosphors and laser spectroscopy.

The kinetics of recombination interaction of luminescence and quenching centers, which leads to nonlinear effects, are considered. Formulas are found which express the dependence of the brightness of steady luminescence on the intensity of the exciting and IR light and also on temperature. The kinetics of luminescence quenching is analyzed with regard to the pair correlation of particles, occurring as a result of the fact that electrons and holes have finite length of free path. A number of problems related to interpretation of experimental facts found as a result of luminescence investigations is considered. The main characteristics of a nonselective IR-SHF radiation field detector, based on the use of crystal-phosphors having high temperature sensitivity, are presented.

The problem of light absorption in the presence of the "self-transparency" phenomenon in ruby is considered theoretically. The calculation is made with regard to degenerate transitions linked by a common level.

The collection is intended for specialists in the field of solid-state physics and quantum electronics.

CONTENTS Page

6521
CSO: 1862

SUPERCONDUCTIVITY

PROBLEMS OF APPLIED SUPERCONDUCTIVITY

Moscow VOPROSY PRIKLADNOY SVERKHPROVODIMOSTI (TRUDY ORDENA LENINA FIZICHESKOGO INSTITUTA IMENI P. N. LEBEDEVA AKADEMII NAUK SSSR) in Russian Vol 121, 1980 pp 2, 179

[Annotation and Table of Contents from the collection edited by Academician N. G. Basov, Izdatel'stvo Nauka, 1,400 copies, 180 pages]

[Text] Papers devoted to development of superconducting magnetic systems (SPMS) not fully stabilized in the thermal relationship are presented in the collection; mechanical stresses in the SPMS winding and their effect on the critical parameters of superconductivity are considered. Processes of energy input and formation of the electromagnetic avalanche upon transition to the normal state in a superconducting solenoid with internal shielding are analyzed. The results of investigating superconducting switches and low-vaporizing current leads are presented. A stabilized power supply source and also a liquid helium level meter are described. The measured characteristics of some superconducting alloys are presented.

The edition is intended for physicists specializing in the field of developing superconducting magnetic systems.

CONTENTS Page

6521
CSO: 1862

- END -